SiAl Composite Feedhorn Arrays for Astrophysical Applications: Cryogenic Material Properties

Aamir M. Ali,[1,2,a)] Thomas Essinger-Hileman,[3] Tobias Marriage,[2] John W. Appel,[2] Charles L. Bennett,[2] Matthew R. Berkeley,[4,3] Berhanu Bulcha,[3] David T. Chuss,[5] Sumit Dahal,[2,3] Kevin L. Denis,[3] Karwan Rostem,[3] Kongpop U-Yen,[3,6] Edward J. Wollack,[3] and Lingzhen Zeng[7]

[1)]*Dept. of Physics, University of California - Berkeley, Berkeley, CA, USA 94720*
[2)]*Dept. of Physics and Astronomy, Johns Hopkins University, Baltimore, MD, USA 21218*
[3)]*NASA Goddard Space Flight Center, Greenbelt, MD, USA 20771*
[4)]*The Catholic University of America, Washington, DC, USA 20064*
[5)]*Villanova University, Villanova, PA, USA 19085*
[6)]*Faculty of Engineering, Chulalongkorn University, Bangkok, Thailand 10330*
[7)]*Harvard-Smithsonian Center for Astrophysics, Boston, MA, USA 02138*

(Dated: 8 December 2021)

A study investigating the physical properties and use of SiAl composite CE7 for the packaging of silicon bolometric detectors for millimeter-wave astrophysical applications at cryogenic temperatures is presented. Existing interfaces to such detectors are typically made either of ductile metals or micro-machined silicon. As a composite of Si and Al, we find CE7 exhibits properties of both in ways which may be advantageous for this application. This exploration of the physical properties of CE7 reveals: a) superconductivity below a critical transition temperature, $T_c \sim 1.2$ K; b) a thermal contraction profile much closer to Si than metal substrates; c) the relatively low thermal conductivity anticipated for a superconductor, which can be improved by Au-plating; and d) the feasibility of machining mechanical features with tolerances of $\sim 25\,\mu$m. We further discuss the use of CE7 in the Cosmology Large Angular Scale Surveyor (CLASS) telescope array, which deployed CE7 in several of its detector focal planes.

I. INTRODUCTION

Advancements in detector technologies have led to the fabrication of arrays of millimeter-wave monolithic detectors on wafers up to 150 mm in diameter[1]. Two practical challenges to their use in astrophysical applications are 1) effective packaging in the cryogenic environments necessary to achieve stable, low-noise performance, and 2) an effective method of coupling light onto the detector.

It is generally difficult to mate silicon devices to metallic substrates[2] in cryogenic settings due to the significant mismatch in thermal contraction between silicon and typical metals. Mating large silicon wafers to metal is highly nontrivial and comes with a risk of damaging or destroying the silicon device. Using silicon itself as the packaging substrate is complicated by the time and resources required to fabricate the alignment features, coupling structures, and feedhorn profiles as a platelet stack[3,4]. Some interfaces to Si are made with a Nickel-Iron metal alloy known as 'Invar' (FeNi36), which shows minimal thermal contraction[5,6]. Invar has the disadvantage of being ferromagnetic, which can negatively impact superconducting detector technologies and their associated readout systems[7,8], and of being very soft for a metal and comparably more difficult to machine than aluminum or copper.

A proven technique for optical coupling is the use of feedhorns which mate to on-wafer antennas.[2,9] Earlier work demonstrated feedhorns using a profiled smooth-walled synthesis procedure and manufacturing process which demonstrated improved beam symmetry, cross-polarization, and bandwidth relative to the prior art[10]. The use of a smooth wall and monotonic profile allows for efficient, cost-effective fabrication using simpler machining techniques than necessary for corrugated feeds[11–13] or silicon platelet arrays[4,11] typically used in millimeter-wave radio astronomy applications.

Presented here is a study of the Controlled Expansion 7 (CE7) SiAl composite in particular its cryogenic material properties, to address the general challenges of packaging silicon devices. We also report on the development of waveguide interface plates and smooth-walled feedhorn arrays made of CE7 for millimeter-wave detectors. CE7 is a proprietary material of Sandvik Osprey[14] consisting of 70% silicon and 30% aluminum, exhibiting a comparable coefficient of thermal expansion (CTE) to Si from room to cryogenic temperatures. The alloy is formed by atomization of its constituents and spray-casting to form solid silicon–aluminum that undergoes rapid solidification[15,16], which results in a uniform and isotropic grain structure. In-house Osprey fabrication capabilities enable the machining of pieces with detailed features to high tolerances. Prior application of this class of material in electronic packaging can be found in e.g. Jacobson et al. 1998[17] or Liu et al. 2020[18].

This report will discuss several CE7 material properties (section II), highlighting those that make it particularly advantageous for the cryogenic packaging of silicon devices. Details of experimental verification of these properties are presented. We describe the machinability of the material as explored in the fabrication of baseplates and feedhorn arrays for millimeter-wave detectors, in particular as deployed in the CLASS[19] cosmic microwave background experiment[20]. We also present a demonstration of the limits of the machinability of fine features (~ 100 microns) through production of a ring-loaded impedance-matching structure (see Figure 7). This pa-

[a)]The author to whom correspondence may be addressed: aamir.mohammed.ali@gmail.com

per expands further upon work first presented in a conference proceedings.[21]

II. MATERIAL PROPERTIES

As a composite, CE7 either maintains properties of silicon and aluminum or a combination of the two. Its room-temperature properties are well documented and are summarized in Table I. It is a dull gray, ceramic-like composite, which is brittle, as indicated by the fact that the yield strength and ultimate tensile strength are essentially identical. It is lightweight and has similar Young's and rigidity moduli as Si. It is composed of interwoven continuous Si and Al phases, with a typical grain size $\sim$10 µm, as determined from lapped samples imaged via scanning electronic micrography (SEM, shown in Figure 6).[35]

To the best of our knowledge, the $\lesssim$ 4 K properties of CE composites relevant to the packaging of very low-temperature silicon detectors have not been reported in the literature. Several cryogenic properties of CE7 were measured in an HPD Olympus[36] adiabatic demagnetization refrigerator (ADR) cryostat. All temperature measurements were made using calibrated thermometers. Diode thermometers were used at temperatures above 4 K, while below 4 K either a calibrated germanium resistance temperature sensor (GRT) or calibrated Ruthenium Oxide (ROX) thermometers were used[37]. Strain gauge and material resistances were read out using a Lake Shore LS370 resistance bridge.

A. Resistivity and Superconductivity

Cryogenic NbTi wire was soldered[38] in a 4-lead configuration across a 'serpentine' sample of CE7 (cross sectional area 1.82 mm^2, length 1982 mm) with 26 meanders (manufactured by wire electrical discharge machining). The sample was mounted and heat sunk with 2 copper bars (on opposite sides of the sample) to the ADR cold stage (Figure 1).

Measurements of the resistivity were made continuously in 10 second steps as the sample cooled from room temperature to 2.5 K. At room temperature, the resistivity measured $\rho =$ 4.40 µΩ · m and decreased monotonically with temperature until $\sim$ 20 K, below which it settled to a normal resistivity of 0.50 $\pm$ .03 µΩ·m. As such, the residual-resistivity ratio (RRR) of the sample was approximately 9, consistent with that of a relatively pure Al[39].

After the sample was cooled to the ADR base temperature, the temperature was PID servo controlled in 5 mK steps from 65 mK to 2.5 K back down to 65 mK 25 times. The resistance of the sample was recorded along with the temperature as measured by the GRT. The complete set of measurements of the 25 sweeps were averaged and binned at 5 mK intervals as shown in the right panel of Figure 1. A transition from normal resistivity to a superconducting state was observed with a width of roughly 90 mK, from 1.15 K to 1.24 K. Defined as the point where the resistivity is half of the normal resistivity, the critical temperature is measured to be $T_c = 1.190 \pm .005$ K, remarkably close to the critical temperature of Al at 1.18 K[40]. This result suggests that a portion of the Al in the composite exists in a continuous lattice in a relatively pure state without appreciable alloying, as expected due to the solubility of Si in Al[41].

B. Thermal Contraction

A Vishay WK-06-062AP-350[44] strain gauge was calibrated from room temperature to 4K and epoxied to a 6.35 cm square sample of CE7 (thickness 6.25 mm) by PCM Measurements.[45] A measurement of the linear thermal contraction of CE7 (Figure 2) was performed over a range of 300 K down to 4 K. The fractional linear contraction was constrained to be less than 0.001. Figure 2 presents measurements of the fractional contraction overlaid with 1) measurements of Si contraction as performed by Lyon et al.[42] to cryogenic temperatures, and 2) curves of the contraction of Al, Cu, and invar, using polynomial fits to experimental data from the NIST cryogenic materials database[43]. To 4 K, CE7 is measured to contract somewhat more than invar, alumina[30] or silicon, but significantly less than metals such as Cu or Al (see Table I). The Si-Al composition seems to account for the observed contraction: a simple geometric mean of the contraction of 70% Si and 30% Al (as might be expected from e.g. the logarithmic law of mixing[46]) gives a predicted contraction of $\sim$ .00095, very close to the observed contraction of CE7.

C. Thermal Conductivity

Below the transition temperature, thermal transport in a superconducting media is exponentially suppressed[47]. As a result, the CE7 composite is anticipated to become a relatively poor thermal conductor below the observed critical temperature of 1.19 K. The thermal conductivity was measured using a rectangular bar (approximately 10 cm $\times$ 1 cm $\times$ 1 cm) mounted on the bottom to the 100 mK ADR cold stage, and a heater of known resistance mounted on the top to supply thermal power. The thermal gradient was measured using 5 calibrated ROX thermometers screwed into the CE7 distributed evenly along the bar (1.66 cm separation). The power applied to the sample varied between 0 and 14 µW, yielding data on the thermal conductivity of CE7 at temperatures below 500 mK. Given the low conductivity of CE7, an identical bar was prepared and plated with gold (7 µm electroless nickel baselayer followed by 3.8 µm soft gold[48]) and analogously measured in order to verify that gold plating improved the conductivity as expected (see section III A for details of plating procedure).

Below 500 mK, the relationship between the temperature of a thermometer on the unplated CE7 sample and the applied power is well described by a standard power law[34,49] as:

$$P = \frac{A}{L}\sigma\left(\left(\frac{T_a}{T_0}\right)^n - \left(\frac{T_b}{T_0}\right)^n\right) \quad (1)$$

TABLE I. CE7 thermal, mechanical, and electrical properties, with comparisons to Si[22], Al 6061[23], Cu[24], and alumina (Al_2O_3)[25,26]. Measurements of CE7 mechanical properties were performed at room temperature by Sandvik Osprey[27]. Values in bold were measured in this report. Note that the similar values of the CE7 yield strength and ultimate tensile strength indicate the brittleness of the material, with minimal plastic deformation, a property inherited from silicon.

	CE7	Si	Al-6061	Cu	Al_2O_3
Ultimate tensile strength (MPa)	∼100	7000	310	220	260
Yield strength (MPa)	110	7000	276	33.3	69
Young's modulus (GPa)	129.2	112.4	68.0	110	370
Rigidity modulus (GPa)	51.6	43.9	25.0	46.0	140
Poisson's ratio	0.26	0.28	0.36	0.343	0.22
Density (g/cm^3)	2.43	2.533	2.699	8.63	3.90
Superconducting T_c (K)	**1.19**	N/A	1.18[28]	N/A	N/A
293 K ⇒ 1 K Contraction ($\times 10^4$) [a]	**<10**	2.16	41.4	32.6	5.16
Thermal Conductivity 300 mK (W / m · K)[b]	**0.005**[c]	- [d]	0.85	$\gtrsim$ 8.0	0.01
Resistivity 1.5 K (μΩ · m)[e]	**0.50**	- [f]	1.5×10^{-2}	1.6×10^{-4}	-[g]
Resistivity 300 K (μΩ · m)	**4.40**	170[h]	3.99×10^{-2}	1.70×10^{-2}	1×10^{20}

[a] Values for the linear thermal contraction calculated from 293 K to 1 K are taken from White et al., 1993[29], while the value for alumina (Al_2O_3) is taken from Wachtman et al., 1962[30].
[b] The thermal conductivity of Al 6061 and OFHC copper (RRR=100) is taken from Woodcraft,[31] while the conductivity of alumina is taken from the review by Simon et al. 1994[32].
[c] Unplated CE7. Gold-plated CE7 conductivity is higher.
[d] No value is given for the thermal conductivity or resistivity of Si because at cryogenic temperatures as these parameters can range from those encountered in insulators to metals depending on the purity and doping of the material[33].
[e] Measurement of resistivity of Cu and Al 6061 taken from the review by Duthil[34] and assumes OFHC copper with RRR=100.
[f] See footnote d
[g] Alumina has a resistivity of 2×10^{12} Ω·m at room temperature which increases monotonically with decreasing temperature (see, e.g., Simon et al. 1994[32]).
[h] The resistivity of a semiconductor such as Si depends strongly on the material's temperature, doping, and impurity concentrations.

with P the power on the heater, L the length between two thermometers, A the area between two thermometers, proportionality constant σ, T_a and T_b the thermometer temperatures, T_0 a pivot scale of $1K$, and n the exponent of the power law (figure 3). A fit of the temperature vs. power data to equation 1 gives values of

$$n = 4.89 \pm .07 \tag{2}$$

$$\sigma = 0.191 \pm .007 \frac{\text{Watts}}{\text{m}} \tag{3}$$

for the power law exponent and σ. A pair-wise removal of any given pair of T_a and T_b thermometers for $(a,b) \in \{1,2,3,4,5\}$ was performed to ensure consistency and check for outliers. T3 was found to be systematically miscalibrated, but all other pairs were considered and fit to equation 1. A power law exponent n = 4.89 is derived from the experimentally observed response. Physically, n = 5 is commonly associated with electron-phonon coupling[50].

Two common operating temperatures for low-background astrophysical millimeter wave detectors are 300 mK and 100 mK, corresponding to the usual base temperatures of He adsorption refrigerators for the former and ADRs or dilution refrigerators (DRs) for the latter. The measured thermal conductivity of bare CE7 at 300 mK is approximately 0.005±0.001 $\mathrm{W/m \cdot K}$, but no value is available at 100 mK since we were unable to cool the bare CE7 sample below 200 mK. The equivalent thermal conductivity for Au-plated CE7 is 0.02± 0.005 $\mathrm{W/m \cdot K}$ at 300 mK and 0.006±0.002 $\mathrm{W/m \cdot K}$ at 100 mK. The observed increase in conductance of the sample with gold electroplating is accounted for given the thickness deposited if the gold had a RRR∼5,[51] a plausible value in the presence of impurities in the plated gold.

D. Room Temperature Microwave Surface Resistance

The room-temperature electrical surface resistance of CE7 at microwave frequencies was measured at frequencies of $77-110$ GHz using circular waveguide sections. An Agilent PNA-X vector network analyzer (VNA) measured scattering matrix parameters (See Figure 4) of CE7 waveguide samples. Two samples were measured with lengths of 7 mm and 25 mm and waveguide diameter 2.98 mm. The samples were measured before and after gold plating, as described in more detail below. The measurement was made using constant waveguide cutoff rectangular (WR-10) to circular waveguide transitions.[52] The VNA was calibrated at the rectangular guide flange interface with a custom WR10 thru-reflect-line (TRL) calibration set. A reference measurement with the transitions[52] directly connected with no intervening CE7 circular waveguide section is used to correct the average loss from the waveguide transitions. The circular guide has two polarizations and misalignment can lead to excitation and the observation of trapped modes in the guide between the two transitions.[53] These resonances provide a measure of the mode coupling,[52] and these portions of the measured response are not used in the subsequent analysis.

Because of the symmetric nature of the measurement, the loss for a given configuration is characterized separately for

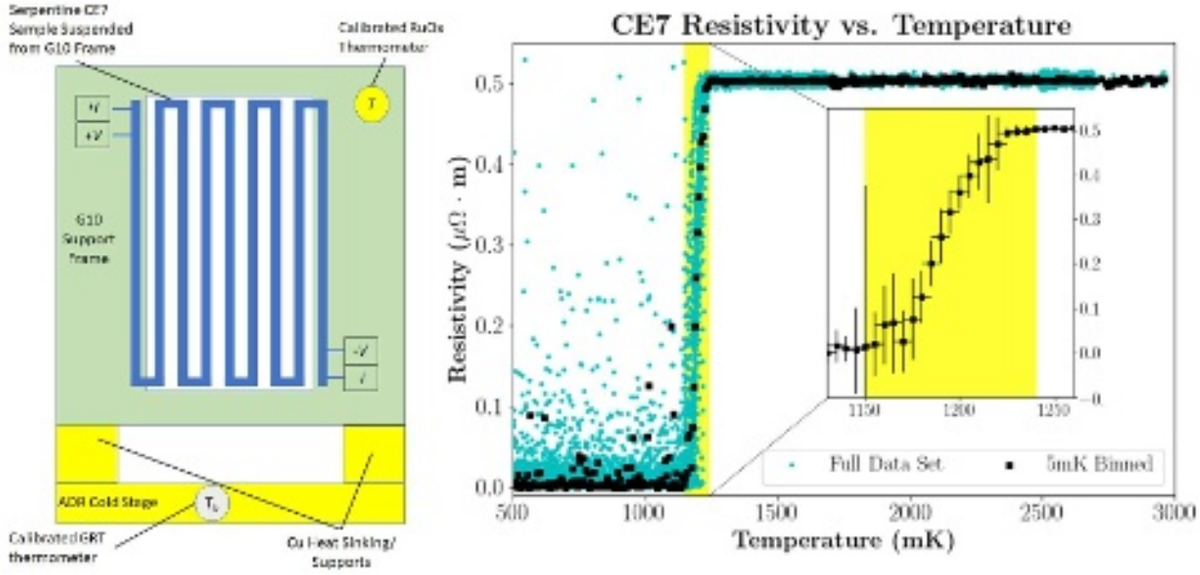

FIG. 1. *Left:* Schematic representation of CE7 resistivity test apparatus. Four leads were soldered to a serpentine meander of CE7 suspended from a G10 frame for electrical isolation. The resistivity of the sample was continuously measured from room temperature to 65 mK. The temperature of the sample was taken from a calibrated RuOx thermometer mounted on the G10 frame, which was found to closely track the bath temperature (T_b) of the ADR cold stage. *Right:* Measurements of the resistivity of CE7 at cryogenic temperatures, with the full data set in cyan, and the measurements averaged in 5 mK bins in black. Note the superconducting transition with central critical temperature $T_c = 1.19$ K, very close to the expected superconducting transition of Al around 1.18 K. These figures are updated from Ali et. al., 2018[21]

power coming from port 1 and port 2

$$\begin{aligned} L_1 &= 1 - |S_{11}|^2 - |S_{21}|^2 \\ L_2 &= 1 - |S_{22}|^2 - |S_{12}|^2, \end{aligned} \tag{4}$$

and we take as our best estimate of the loss the average of these two values, $\bar{L} = (L_1 + L_2)/2$. We estimate systematic error in our measurement to be at the 5% level based on consistency of L_1 and L_2, driven by error in our reference plane correction.

Then given a measured loss, the surface resistance of the measurement is calculated from the standard formula for the fundamental TE_{11} mode in circular waveguide

$$\alpha_c = \frac{R_s}{ak\eta\beta}\left(k_c^2 + \frac{k^2}{1.841^2 - 1}\right) \text{[Np/m]}, \tag{5}$$

where R_s is the surface resistance, a is the waveguide radius (2.98 mm in our case), $k = 2\pi/\lambda$ is the wavenumber given wavelength λ, $\eta = 377\ \Omega$ is the impedance of free space, $k_c = 1.841/a$ is the waveguide cutoff, and $\beta = \sqrt{k^2 - k_c^2}$. The factor 1.841 is particular to the TE_{11} mode.[54] For a homogeneous material, the surface resistance can be related to the bulk conductivity through $R_s = \sqrt{\omega\mu_0/(2\sigma)}$, where $\omega = 2\pi c/\lambda$, c is the speed of light in vacuum, and σ is the bulk conductivity in S/m.

We take as our best estimate of the conductive loss in the waveguide the difference between the 25 mm measured loss and the 7 mm measured loss after correcting for the loss from the reference measurement, and equate this with the conductive loss from 18 mm of CE7 waveguide. This corrects for average loss between the calibration reference plane and the circular-to-square transitions, as well as that from adding an additional waveguide flange in changing between the reference and the CE7 tests. We average the measured loss over the frequency range 77-90 GHz, amounting to 3% and 8% loss for the 7 mm and 25 mm waveguide lengths, respectively. We measure a waveguide loss of approximately 1.4 Np/m, corresponding to a surface resistance of 0.61 Ω per square.

If CE7 were a homogeneous material, this would imply a bulk conductivity of 8.9×10^5 S/m (bulk resistivity of $1.1\,\mu\Omega\cdot$m). We note that the associated electromagnetic skin depth for a non-magnetic material,

$$\delta = \sqrt{\frac{2}{\mu_0\sigma\omega}}, \tag{6}$$

is 1.7 μm at $\nu = 100$ GHz. Here $\mu_0 = 4\pi \times 10^{-7}$ H/m is the permeability of free space, σ is the conductivity, and $\omega = 2\pi\nu$ is the angular frequency. This skin depth is smaller than the grain size in the material of approximately 10 μm.

Treating the bulk material properties in the microwave as homogeneous is thus not valid, which may explain why the microwave loss is a factor of 4 lower than expected from our measurement of room-temperature DC resistivity, $4.40\,\mu\Omega\cdot$m. The microwave loss and DC resistivity are higher, by factors of approximately 10 and 100, respectively, than that of relatively pure aluminum. At the same time, the RRR value of 9 measured in our sample (see Section II A) is similar to a bulk metallic aluminum. These facts combined

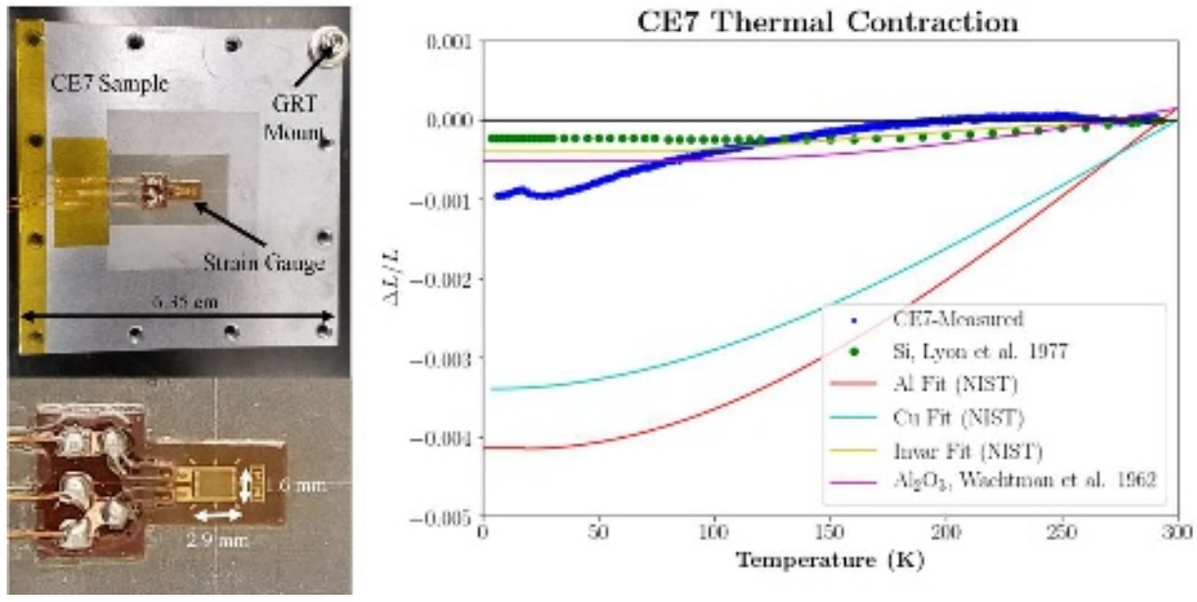

FIG. 2. *Top Left:* A calibrated strain gauge affixed to a sample of CE7, which was mounted directly to an ADR cold stage. The variation in CE7 appearance is the result of a roughening of the area to improve strain gauge adhesion. A GRT thermometer screwed into the CE7 sample measured the temperature, while the strain gauge measured the fractional contraction of the CE7 sample. *Bottom Left:* Zoom in of strain gauge. *Right:* Fractional contraction of CE7 as measured with a calibrated strain gauge (blue), with overlays of measurements of Si contraction as performed by Lyon et al. 1977[42] (green circles), and contraction curves of various substrates determined by the National Institute of Standards and Technology[43] such as aluminum (red), OFHC copper (black), and invar (gold). A contraction curve of alumina is taken from Wachtman et al., 1962[30]. These figures are updated from Ali et. al., 2018[21]

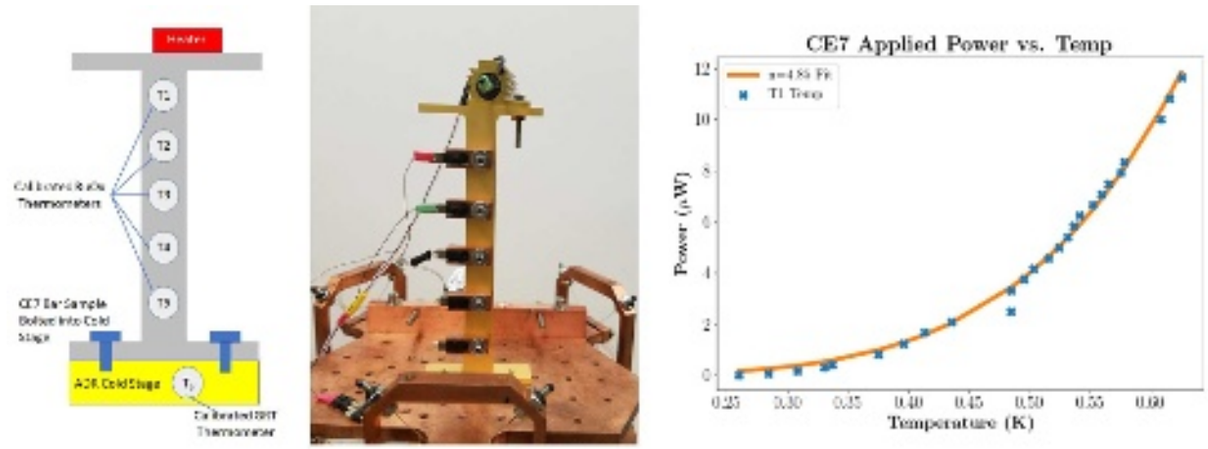

FIG. 3. *Left:* Schematic representation of CE7 thermal conductivity measurement. The bottom of a bar of CE7 was screwed to the cold stage of an ADR (thermal sink), while a heater was screwed to the top of the bar. Along the bar, 5 RuOx thermometers were screwed directly into the CE7 to measure a temperature gradient induced by the heat load. *Center:* A photograph of an Au-plated CE7 bar thermal conductivity test setup, as described. Measurements of the thermal conductivity were performed over multiple cooldowns on both bare and Au-plated CE7 bars. *Right:* Measurements of the temperature of T1 at various applied powers, versus a predicted temperature based on a fit of the thermal conductivity using $n = 4.85$ per the fit in equation 1. This analysis and resultant figures are updated from Ali et. al., 2018[21]

indicate that the DC currents carried in the CE7 may largely travel through a lacework of relatively pure aluminum that makes up a small fraction of the volume of the material. In the microwave, the behavior is more complicated as the fields will interact with a larger volume of the composite Si/Al alloy, which has heterogeneous material properties at some of the length scales of interest.

The same samples were subsequently gold plated to validate our measurement methodology and test the efficacy of plating in improving microwave loss. Measurements of

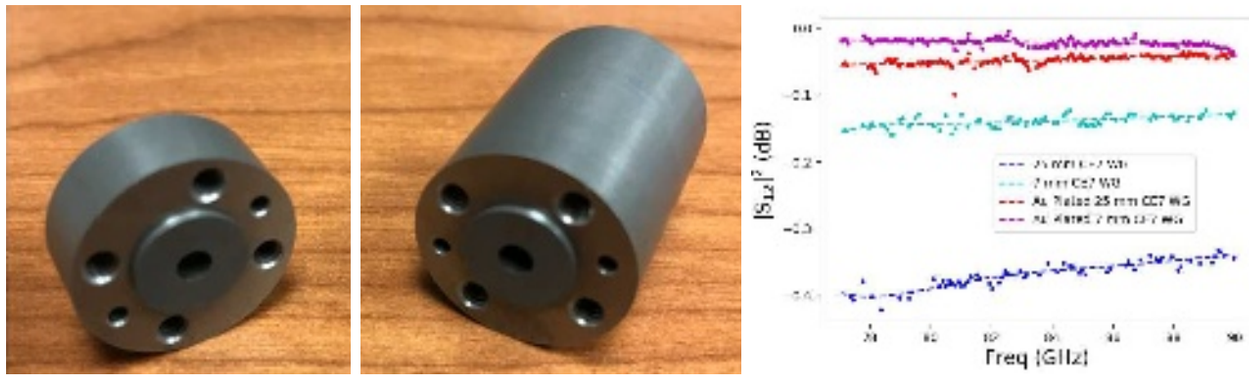

FIG. 4. *Left:* Photograph of the 7 mm long CE7 waveguide part for testing. *Middle:* Photograph of the 25 mm long CE7 waveguide part for testing. *Right:* Measured transmission $|S_{12}|^2$ in dB from vector network analyzer measurements of CE7 waveguide parts over frequency range used for the analysis. The plot for $|S_{21}|^2$ is nearly identical. The solid lines show the measured spectrum, while the dashed lines show the fifth-order polynomial fit to the data.

waveguide loss for the plated samples are broadly consistent with the bulk properties of gold. Once again, we use the difference between the plated samples to infer the loss for 18 mm of waveguide. We measure a waveguide loss of 0.17 Np/m, from which we estimate the surface resistance of the gold plating to be 0.07 Ω per square and the bulk conductivity to be 7.6×10^7 S/m. This is in reasonable agreement with the electrical conductivity of bulk gold, which has typical values around 4×10^7 S/m.[55]

III. CE7 DETECTOR INTERFACE PLATES AND FEEDHORNS

The results presented in section II have implications for the suitability of CE7 for precision waveguide interfaces and feedhorn arrays which are encountered in cryogenic sensors employed for astrophysical applications. Based on these results, CE7 is employed as the packaging material for detectors in 3 of the 4 telescopes in the Cosmology Large Angular Scale Surveyor (CLASS) Cosmic Microwave Background (CMB) telescope array[7,56]. For the two CLASS 90 GHz telescopes (the first of which is deployed), interface plates with circular waveguides are made of CE7 and couple/align the detector array wafers to copper feedhorns and provide the base for the overall structure of the detector modules (Figure 5). For the CLASS dichroic 150/220 GHz telescope, the detector arrays are mounted directly to a feedhorn array machined out of a monolithic block of CE7. The ensuing discussion will address the suitability of CE7 for Si packaging, leveraging both the measurements made above as well as the practical experience gained by its use in the CLASS telescopes. Relevant comparisons are made to other substrates.

A. Thermal Conductivity and Gold Plating

Due to the low thermal conductivity of CE7 at cryogenic temperatures, it was found necessary to gold plate parts to provide a sufficiently conductive path to cool the CLASS detectors to the desired base temperature of <100 mK. The process that we found successful for plating the CE7 substrate was the application of a 7 µm electroless nickel adhesion layer followed by 3.8 µm high-purity gold layer. The use of a non-magnetic Ag adhesion layer for the CE7 substate was also investigated. The Ag plating procedure was found to be less reliable due to the occurrence of blistering and resulted in the selection of Ni for the CE7 adhesion layer.

The Transition Edge Sensor (TES) detectors were characterized both with the Ni underplate and without to see if the magnetic material shifted the detector properties (most notably, the T_c of the TES), but no evidence of any such shift was detected at the 3 mK level. It is possible that this is the result of the particulars of the CLASS detector implementation[57], for instance the incorporation of superconductors at select locations to shield the devices from spurious magnetic fields, so it is possible that this may vary in other applications.

After plating, the part tracked the temperature of the cold stage within 10 mK, and it was determined that the package thermal bus was sufficiently conductive for our purposes. In comparison to other choices for cryogenic packaging, Cu, a normal metal, is more suitable from the perspective of thermal conductivity than a bulk superconductor below its transition temperature where thermal transport is exponentially suppressed[47]. In practice, Si, invar, and alumina all have relatively low thermal conductivities and are often plated or heat sunk using gold ribbon bonding and high conductivity interface materials when heat removal from the package and thermal gradient mitigation are driving implementation considerations.

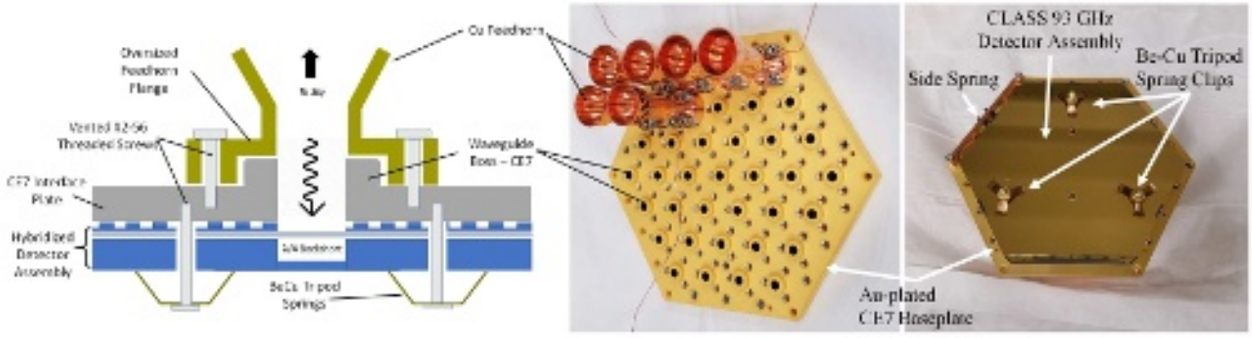

FIG. 5. CLASS 90 GHz Au-plated CE7 waveguide interface plate, mating CLASS 90 GHz detector assembly with Cu feedhorns *Left:* Schematic representation of interface between detector assembly, CE7 interface plate, and Cu feedhorn. The interface plate consists of an array of cylindrical boss extrusions housing the waveguides to interface with the Cu feedhorns. A corresponding feature at the base of the Cu feedhorns is oversized so as to 'grab' the cylindrical boss with the cryogenic contraction of the Cu. The feedhorns are screwed into threaded #2-56 holes machined in the CE7 plate with inserted helicoils. The detector assembly is vertically constrained simply with the use of three Be-Cu spring clips screwed into threaded #2-56 holes in the CE7 plate. *Center* Photograph of CE7 interface plate, partially populated with Cu feedhorns. *Right* A CLASS 90 GHz detector assembly is mounted onto the CE7 interface plate. Waveguide alignment (*x*-*y* plane) is accomplished by means of 2 alignment pins situated in the baseplate which are designed to press against a flat edge and corner groove in holes in the detector wafer. A side mounted Be-Cu spring applies between .25-0.5 N of force to press the alignment pins against the hole features. This constrains the rotation and translation of the wafer ensuring waveguide to antenna-pair alignment. These figures were published prior in Ali, 2017[7] and Ali et. al., 2018[21]. The mounting scheme for the CLASS 150/220 dichroic detector is similar, less the complication of mating feedhorns with an interface plate, as the monolithic CE7 feedhorn array mates with the detector directly.

B. Superconductivity and Magnetic Shielding

Because CE7 superconducts below 1.2 K, it will affect magnetic fields by pinning and/or excluding magnetic flux. This behavior is necessary to consider when incorporating CE7 into a detector and readout system. Trapped flux can locally enhance DC magnetic fields, which could adversely affect some detectors. The transition edge sensor (TES) bolometers and superconducting quantum interference device (SQUID) amplifiers commonly employed in millimeter-wave detector assemblies are both susceptible to magnetic fields. In the CLASS implementation, no measurable change in T_c or response from the presence of the CE7 or the ferromagnetic Ni adhesion layer (see Section III A) was observed. In the CLASS detector wafer implementation, there is, by design, electromagnetic separation between magnetically active materials, and intervening superconducting ground planes are used in the micromachined detector subassembly to mitigate these considerations[58]. No measurable change in Tc or response from the presence of the CE7 or the ferromagnetic Ni adhesion layer (see Section III A) was experimentally observed. The presence of nickel warrants attention to detail to limit its potential impact on microwave circuitry (see for example[59,60]) and magnetically sensitive elements. In similar astrophysical scenarios, magnetic fields are typically shielded through the combined use of high magnetic susceptibility metals and superconductors[61,62], and it is likely that the superconductivity of the CE7 could be of benefit in this context, particularly in the rejection of AC fields.

C. Thermal Contraction

Although the contraction of CE7 is greater than pure Silicon, it is a much closer match than metallic substrates, and is acceptable given the gain in fabrication ease vs. silicon (section III D). CLASS detectors were mounted kinematically with a BeCu side spring clip that presses a V-groove in the wafer against one pin (leaving rotational freedom) and a flat in the wafer against a second pin to set the angle. This allowed alignment of the wafer to the CE7 within machining tolerances of 20 µm. Assembled modules have been warmed/cooled over multiple cycles (>10) with no evidence of misalignment or other failure. Thermal contraction needed to be accounted for primarily at interfaces where the CE7 would mate to metals, rather than to the detector silicon itself, although for higher precision alignments, the differential contraction may need to be accounted for.

The thermal contraction of CE7 is far less than comparable metals, and is slightly higher than alumina, invar, or Si. We have found CE7 to be a sufficiently close match at the tolerances of interest to not drive a choice to the latter three substrates: alumina and Si were down-selected due to machinability (Section III D) and cost concerns, while invar was rejected largely due to magnetic concerns (Section III B).

D. Fabrication

CE7 is more easily machined than ceramics or silicon, but not as easily machined as typical metals. The characteristic Si grain size of the composite is of order 10 µm. Structures approaching this size are typically difficult to machine

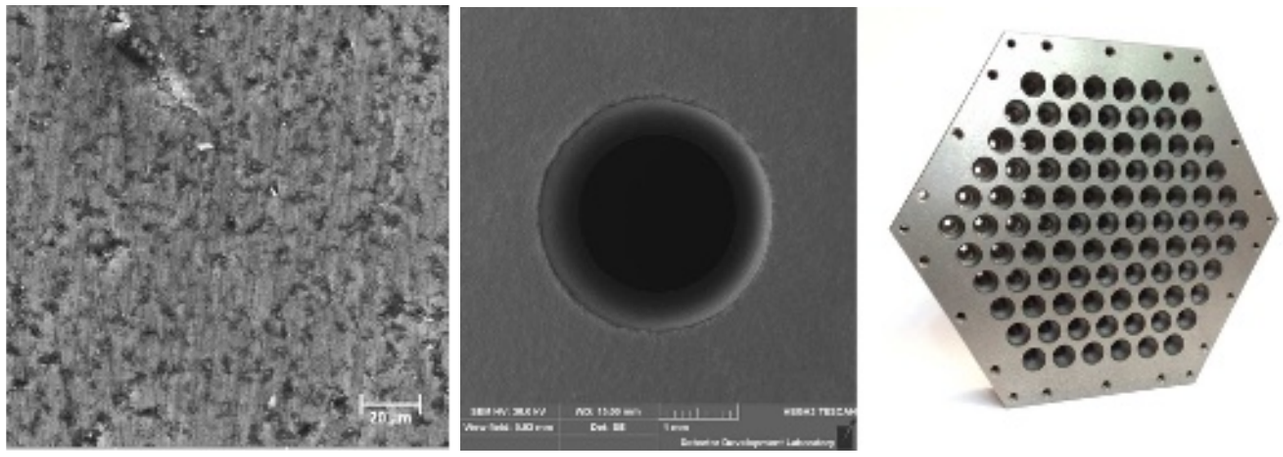

FIG. 6. *Left:* Scanning electron migrograph (SEM) of CE7, showing the $\sim 10\,\mu$m grain size. *Middle:* SEM of 90 GHz CLASS detector baseplate waveguide fabricated out of CE7. *Right:* Photograph of a 91-element CE7 feedhorn array for 150/220 GHz CLASS focal plane. This array was machined with conservative spaces between the tops of feedhorns. These figures are updated from Ali et. al., 2018[21]

because fractures occur in the material at grain boundaries; however, parts have been produced with surface finish better than 0.4 µm and flatness better than 5 µm. Sandvik Osprey has demonstrated the ability to machine threaded holes as small as #0-80 (with feature tolerances of the threads of order 10 µm). The waveguides fabricated in the CLASS 90 GHz interface plates held diameter tolerances of $\pm 10\,\mu$m, and the waveguide boss extrusions were fabricated to tolerances of $\pm 25\,\mu$m. Tolerances of $\sim 25\,\mu$m are hard, but doable, while tolerances $\sim 10\,\mu$m are near the edge of capability, and can be achieved with specialized machining techniques, like using precision reamers or plunge electrical discharge machining.

Features approaching a few times the grain size were most successfully machined using a plunge electrical discharge machining process, which avoids placing undue stress on the material during machining. As an example, a ring-loaded impedance-matching section, used to increase the feedhorn bandwidth by improving the return loss at the lower band edge, was successfully machined into a CE7 waveguide section at the base of a feedhorn, as shown in Fig. 7. The ring-loaded structure contained a raised boss 93 µm tall and 208 µm wide. This feature was successfully machined, but features much smaller would be very challenging.

IV. CONCLUSION

We have reported on the cryogenic and microwave material properties of CE7 and commented on the suitability of CE7 for mating to silicon devices in astrophysical settings. In particular, we have: (1) characterized the electrical resistivity from room temperature to 500 mK, which showed a RRR of 9 and a superconducting transition at 1.19 K; (2) measured the thermal contraction to be $\Delta L/L \simeq 0.001$ from room temperature to 4 K; (3) measured bare CE7 and Au-coated CE7 to have thermal conductivities of 0.005 ± 0.001 and 0.02 ± 0.005 $(W/m \cdot K)$ respectively at 300 mK, with the thermal conductivity of the bare CE7 falling below our measurement systematic error below ~ 220 mK; and (4) measured room-temperature microwave surface resistance to be 0.61 Ω per square at 90 GHz, a factor of 4 lower than one would naively infer from room-temperature DC resistivity.

We described the suitability of CE7 for packaging Si in cryogenic contexts. In particular, we recommend plating the CE7 with gold to enhance thermal conductivity or reduce microwave loss where required for a given application. We also fabricated waveguide array interface plates and feedhorn arrays out of CE7 for use in the CLASS CMB telescopes and described the mating procedure, demonstrating CE7 to be a mature and attractive choice for astrophysical instruments.

ACKNOWLEDGMENTS

The authors graciously acknowledge a private gift from Matthew Polk (Johns Hopkins Physics and Astronomy B.S. alum, 1971) which funded much of this investigation, including Aamir Ali for a portion of his graduate studies. We acknowledge the National Science Foundation Division of Astronomical Sciences for their support of CLASS under Grant Numbers 0959349, 1429236, 1636634, and 1654494. CLASS uses detector technology developed under several previous and ongoing NASA grants. Detector development work at JHU was funded by NASA grant number NNX14AB76A. We are also grateful to NASA for their support of civil servants engaged in state-of-the-art detector technologies. T. Essinger-Hileman was supported by an NSF Astronomy and Astrophysics Postdoctoral Fellowship. K. Clavadetscher is acknowledged for sample design and preparation and was funded by a AIP/SPS fellowship.

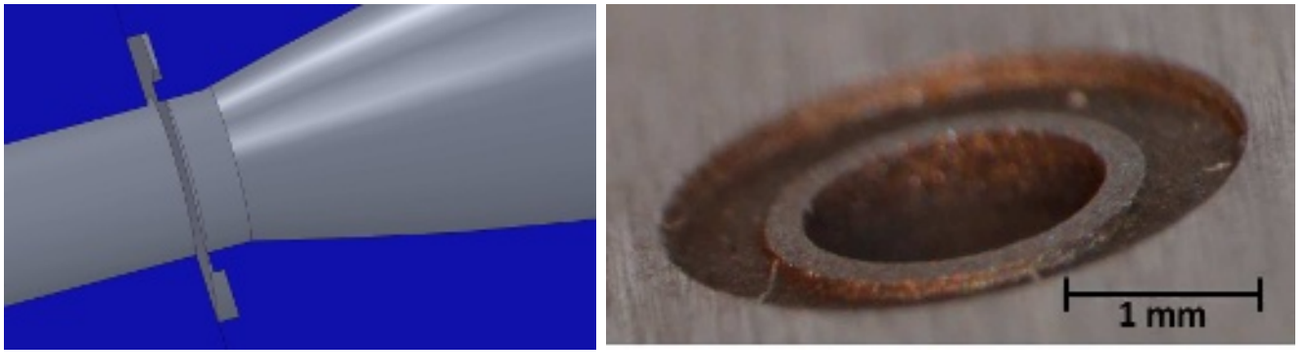

FIG. 7. *Left:* Model of a ring-loaded impedance-matching structure at the base of a feedhorn. *Right:* Photograph of the structure realized in CE7 through a plunge electric discharge machining (EDM) process, showing the ability to manufacture fine features in CE7. These figures are updated from Ali et. al., 2018[21]

DATA AVAILABILITY

The data that support the findings of this study are available from the corresponding author upon reasonable request.

[1]M. H. Abitbol, Z. Ahmed, D. Barron, R. B. Thakur, A. N. Bender, B. A. Benson, C. A. Bischoff, S. A. Bryan, J. E. Carlstrom, C. L. Chang, D. T. Chuss, K. T. Crowley, A. Cukierman, T. de Haan, M. Dobbs, T. Essinger-Hileman, J. P. Filippini, K. Ganga, J. E. Gudmundsson, N. W. Halverson, S. Hanany, S. W. Henderson, C. A. Hill, S.-P. P. Ho, J. Hubmayr, K. Irwin, O. Jeong, B. R. Johnson, S. A. Kernasovskiy, J. M. Kovac, A. Kusaka, A. T. Lee, S. Maria, P. Mauskopf, J. J. McMahon, L. Moncelsi, A. W. Nadolski, J. M. Nagy, M. D. Niemack, R. C. O'Brient, S. Padin, S. C. Parshley, C. Pryke, N. A. Roe, K. Rostem, J. Ruhl, S. M. Simon, S. T. Staggs, A. Suzuki, E. R. Switzer, O. Tajima, K. L. Thompson, P. Timbie, G. S. Tucker, J. D. Vieira, A. G. Vieregg, B. Westbrook, E. J. Wollack, K. W. Yoon, K. S. Young, and E. Y. Young, "CMB-S4 Technology Book, First Edition," (2017), arXiv:1706.02464.

[2]S. M. Simon, J. E. Golec, A. M. Ali, J. McMahon, E. J. Wollack, J. A. Beall, M. Salatino, J. Austermann, N. Zhu, S. R. Dicker, J. Orlowski-Scherer, J. Hubmayr, S. M. Duff, B. Dober, Z. Xu, C. A. Hill, S. M. M. Bruno, S.-P. P. Ho, E. Healy, S. T. Staggs, K. T. Crowley, Y. Li, S. K. Choi, and M. Lungu, "Feedhorn development and scalability for Simons Observatory and beyond," in *Submitted to Proceedings of the SPIE* (2018).

[3]J. W. Britton, J. P. Nibarger, K. W. Yoon, J. A. Beall, D. Becker, H.-M. Cho, G. C. Hilton, J. Hubmayr, M. D. Niemack, and K. D. Irwin, "Corrugated silicon platelet feed horn array for CMB polarimetry at 150 GHz," (2010) p. 77410T.

[4]S. M. Simon, J. Austermann, J. A. Beall, S. K. Choi, K. P. Coughlin, S. M. Duff, P. A. Gallardo, S. W. Henderson, F. B. Hills, S.-P. P. Ho, J. Hubmayr, A. Josaitis, B. J. Koopman, J. J. McMahon, F. Nati, L. Newburgh, M. D. Niemack, M. Salatino, A. Schillaci, B. L. Schmitt, S. T. Staggs, E. M. Vavagiakis, J. Ward, and E. J. Wollack, "The design and characterization of wideband spline-profiled feedhorns for Advanced ACTPol," in *Proceedings of the SPIE, Volume 9914, id. 991416 13 pp. (2016).*, Vol. 9914, edited by W. S. Holland and J. Zmuidzinas (2016) p. 991416.

[5]B. Westbrook, P. A. Ade, M. Aguilar, Y. Akiba, K. Arnold, C. Baccigalupi, D. Barron, D. Beck, S. Beckman, A. N. Bender, F. Bianchini, D. Boettger, J. Borrill, S. Chapman, Y. Chinone, G. Coppi, K. Crowley, A. Cukierman, T. de Haan, R. Dünner, M. Dobbs, T. Elleflot, J. Errard, G. Fabbian, S. M. Feeney, C. Feng, G. Fuller, N. Galitzki, A. Gilbert, N. Goeckner-Wald, J. Groh, N. W. Halverson, T. Hamada, M. Hasegawa, M. Hazumi, C. A. Hill, W. Holzapfel, L. Howe, Y. Inoue, G. Jaehnig, A. Jaffe, O. Jeong, D. Kaneko, N. Katayama, B. Keating, R. Keskitalo, T. Kisner, N. Krachmalnicoff, A. Kusaka, M. Le Jeune, A. T. Lee, D. Leon, E. Linder, L. Lowry, A. Madurowicz, D. Mak, F. Matsuda, A. May, N. J. Miller, Y. Minami, J. Montgomery, M. Navaroli, H. Nishino, J. Peloton, A. Pham, L. Piccirillo, D. Plambeck, D. Poletti, G. Puglisi, C. Raum, G. Rebeiz, C. L. Reichardt, P. L. Richards, H. Roberts, C. Ross, K. M. Rotermund, Y. Segawa, B. Sherwin, M. Silva-Feaver, P. Siritanasak, R. Stompor, A. Suzuki, O. Tajima, S. Takakura, S. Takatori, D. Tanabe, R. Tat, G. P. Teply, A. Tikhomirov, T. Tomaru, C. Tsai, N. Whitehorn, and A. Zahn, "The POLARBEAR-2 and Simons Array Focal Plane Fabrication Status," JLTP **193**, 758–770 (2018).

[6]Y. Nakamura, "The invar problem," IEEE Transactions on Magnetics **12**, 278–291 (1976).

[7]A. M. Ali, *Detectors and Focal Planes for the Cosmology Large Angular Scale Surveyor*, Ph.D. thesis, Johns Hopkins University (2017).

[8]E. M. Vavagiakis, S. W. Henderson, K. Zheng, H.-M. Cho, N. F. Cothard, B. Dober, S. M. Duff, P. A. Gallardo, G. Hilton, J. Hubmayr, K. D. Irwin, B. J. Koopman, D. Li, F. Nati, M. D. Niemack, C. D. Reintsema, S. Simon, J. R. Stevens, A. Suzuki, and B. Westbrook, "Magnetic Sensitivity of AlMn TESes and Shielding Considerations for Next-Generation CMB Surveys," Journal of Low Temperature Physics , 1–10 (2018).

[9]J. Leech, B. K. Tan, G. Yassin, P. Kittara, and S. Wangsuya, "Experimental Investigation of a Low-Cost, High Performance Focal-Plane Horn Array," IEEE Transactions on Terahertz Science and Technology **2**, 61–70 (2012).

[10]Lingzhen Zeng, C. L. Bennett, D. T. Chuss, and E. J. Wollack, "A Low Cross-Polarization Smooth-Walled Horn With Improved Bandwidth," IEEE Transactions on Antennas and Propagation **58**, 1383–1387 (2010).

[11]J. P. Nibarger, J. A. Beall, D. Becker, J. Britton, H.-M. Cho, A. Fox, G. C. Hilton, J. Hubmayr, D. Li, J. McMahon, M. D. Niemack, K. D. Irwin, J. Van Lanen, and K. W. Yoon, "An 84 Pixel All-Silicon Corrugated Feedhorn for CMB Measurements," Journal of Low Temperature Physics **167**, 522–527 (2012).

[12]M. Bersanelli, E. Mattaini, E. Santambrogio, A. Simonetto, S. Cirant, F. Gandini, C. Sozzi, N. Mandolesi, and F. Villa, "A Low-Sidelobe, High Frequency Corrugated Feed Horn for CMB Observations," Experimental Astronomy **8**, 231–238 (1998).

[13]F. D. Torto, M. Bersanelli, F. Cavaliere, A. D. Rosa, O. D'Arcangelo, C. Franceschet, M. Gervasi, A. Mennella, E. Pagana, A. Simonetto, A. Tartari, F. Villa, and M. Zannoni, "W-band prototype of platelet feed-horn array for CMB polarisation measurements," Journal of Instrumentation **6**, P06009–P06009 (2011).

[14]Marketed as Controlled Expansion (CE) Alloys. Sandvik Osprey Ltd. Milland Rd, Neath SA11 1NJ, United Kingdom.

[15]A. G. Leatham, J. S. Coombs, J. B. Forrest, A. J. W. Ogilvy, R. Ross, and L. G. Elias, "Silicon alloys for electronic packaging," United States Patent No. 6312535, Osprey Metals Limited (2001).

[16]A. Leatham and A. Lawley, "The osprey process: principles and applications," International Journal of Powder Metallurgy **29**, 321–329 (1993).

[17]D. M. Jacobson and S. P. Sangha, "A novel lightweight microwave packaging technology," IEEE Transactions on Components Packaging and Manufacturing Technology Part A **21**, 515–520 (1998).

[18]Y. Q. Liu, J. Z. Fan, X. X. Hao, S. H. Wei, J. H. Nie, Z. L. Ma, M. K. Liu, and Y. B. Wang, "Advanced hermetic electronic packaging based on lightweight silicon/aluminum composite produced by powder metallurgy technique," Rare Metals **39**, 1307–1313 (2020).

[19]T. Essinger-Hileman, A. Ali, M. Amiri, J. W. Appel, D. Araujo, C. L. Bennett, F. Boone, M. Chan, H.-M. Cho, D. T. Chuss, F. Colazo, E. Crowe, K. Denis, R. Dünner, J. Eimer, D. Gothe, M. Halpern, K. Harrington, G. Hilton, G. F. Hinshaw, C. Huang, K. Irwin, G. Jones, J. Karakla, A. J. Kogut, D. Larson, M. Limon, L. Lowry, T. Marriage, N. Mehrle, A. D. Miller, N. Miller, S. H. Moseley, G. Novak, C. Reintsema, K. Rostem, T. Stevenson, D. Towner, K. U-Yen, E. Wagner, D. Watts, E. Wollack, Z. Xu, and L. Zeng, "CLASS: The Cosmology Large Angular Scale Surveyor," Proceedings of the SPIE, Volume 9153, id. 91531I 23 pp. (2014). **9153** (2014), 10.1117/12.2056701, arXiv:1408.4788.

[20]We note that CE7 was also later used in the Advanced ACT Low-frequency instrument[64], which was deployed in 2020[65].

[21]A. Ali, T. M. Essinger-Hileman, T. Marriage, C. L. Bennett, S. Dahal, J. W. Appel, K. Rostem, E. J. Wollack, K. U-Yen, B. T. Bulcha, L. Zeng, M. Berkeley, and K. L. Denis, "SiAl alloy feedhorn arrays: material properties, feedhorn design, and astrophysical applications," in *Millimeter, Submillimeter, and Far-Infrared Detectors and Instrumentation for Astronomy IX*, Vol. 10708, edited by J. Zmuidzinas and J.-R. Gao (SPIE, 2018) p. 146.

[22]"Silicon, Si http://www.matweb.com," ().

[23]"ASM Material Data Sheet, asm.matweb.com,".

[24]"Copper, Cu; Annealed, http://www.matweb.com," ().

[25]"Alumina, alpha Al2O3, 99.5%, http://www.matweb.com," ().

[26]Y. Yamano, T. Komiyama, M. Takahashi, S. Kobayashi, K. Nitta, and Y. Saito, "Measurement of surface and volume resistivity for alumina ceramics under vacuum condition," in *Proceedings - International Symposium on Discharges and Electrical Insulation in Vacuum, ISDEIV*, Vol. 1 (2008) pp. 35–38.

[27]Sandvik-Osprey-CE7, "Controlled Expansion (CE) Alloy Products, http://smt.sandvik.com/en/products/ce-alloys," Sandvik Materials Technology (2014).

[28]F. Iida, T. Suzuki, E. Kuramoto, and S. Takeuchi, "Anomalous strain-rate sensitivity of flow stress in superconducting Al and Al-Mg alloys," Acta Metallurgica **27**, 637–647 (1979).

[29]G. K. White, "Solids: Thermal expansion and contraction," Contemporary Physics **34**, 193–204 (1993).

[30]J. B. Wachtman, T. G. Scuderi, and G. W. Cleek, "Linear Thermal Expansion of Aluminum Oxide and Thorium Oxide from 100o to 1100oK," Journal of the American Ceramic Society **45**, 319–323 (1962).

[31]A. L. Woodcraft, "Recommended values for the thermal conductivity of aluminium of different purities in the cryogenic to room temperature range, and a comparison with copper," Cryogenics **45**, 626–636 (2005).

[32]N. Simon and N.J., "Cryogenic Properties of Inorganic Insulation Materials for ITER Magnets: A Review," Tech. Rep. (National Institute of Standards and Technology, Boulder, CO, 1994).

[33]P. Dai, Y. Zhang, and M. P. Sarachik, "Electrical conductivity of metallic Si:B near the metal-insulator transition," Physical Review B **45**, 3984–3994 (1992).

[34]P. Duthil and P, "Material Properties at Low Temperature," eprint arXiv:1501.07100 (2015), 10.5170/CERN-2014-005.77, arXiv:1501.07100.

[35]Confirmed in a personal communication with Robert Ross of Sandvik Osprey. July 4th, 2017.

[36]Model 104 Olympus Cryostat, High Precision Devices (HPD), 4601 Nautilus Ct S Boulder, CO 80301.

[37]All thermometers were from Lake shore Cryotronics, Westerville, OH 43082.

[38]During soldering, the CE7 sample was heated on a hot-plate to 150°C, and soldered using a standard soldering iron at 300°C using a high-purity 97-In 3-Ag solder.

[39]F. R. Fickett, *NBS Technical Publications* (National Bureau of Standards, Boulder, CO, 1982) pp. 1–80.

[40]G. W. Webb, F. Marsiglio, and J. E. Hirsch, "Superconductivity in the elements, alloys and simple compounds," Physica C: Superconductivity and its applications, Volume 514, p. 17-27. **514**, 17–27 (2015), arXiv:1502.04724.

[41]A. Mostafa and M. Medraj, "Binary Phase Diagrams and Thermodynamic Properties of Silicon and Essential Doping Elements (Al, As, B, Bi, Ga, In, N, P, Sb and Tl)," Materials (Basel, Switzerland) **10** (2017), 10.3390/MA10060676.

[42]K. G. Lyon, G. L. Salinger, C. A. Swenson, and G. K. White, "Linear thermal expansion measurements on silicon from 6 to 340 K," Journal of Applied Physics **48**, 865–868 (1977).

[43]J. L. Marquardt and R. Radebaugh, "Cryogenic Material Properties Database," in *11th International Cryocooler Conference* (2000).

[44]Vishay Precision Group, www.vishaypg.com.

[45]Proctor & Chester Measurements Ltd., Warwickshire CV8 2UE UK.

[46]A. H. Sihvola and Institution of Electrical Engineers., *Electromagnetic mixing formulas and applications* (Institution of Electrical Engineers, 1999) p. 284.

[47]P. Duthil, "Material Properties at Low Temperature," arXiv e-prints , arXiv:1501.07100 (2015), arXiv:1501.07100 [physics.acc-ph].

[48]Nominal thickness of 7 µm electroless nickel adhesion layer and 4 µm gold plate per ASTM B 488 (https://www.astm.org/Standards/B488.htm) Type III (99.9% gold) Grade A (Knoop hardness of 90 or less) were used throughout this work.

[49]M. Newman, "Power laws, pareto distributions and zipf's law," Contemporary Physics **46**, 323–351 (2005), https://doi.org/10.1080/00107510500052444.

[50]F. C. Wellstood, C. Urbina, and J. Clarke, "Hot-electron effects in metals," Physical Review B **49**, 5942–5955 (1994).

[51]H. M. Rosenberg, "The Thermal Conductivity of Metals at Low Temperatures," Philosophical Transactions of the Royal Society A: Mathematical, Physical and Engineering Sciences **247**, 441–497 (1955).

[52]E. Wollack, "TCHEBx: Homogeneous stepped waveguide transformers," NRAO EDTN Technical Note **176** (1996).

[53]M. A. Morgan and S. Pan, "Graphical prediction of trapped mode resonances in sub-mm and thz waveguide networks," IEEE Transactions on Terahertz Science and Technology **3**, 72–80 (2013).

[54]D. M. Pozar, *Microwave engineering; 3rd ed.* (Wiley, Hoboken, NJ, 2005).

[55]J. R. Sambles, K. C. Elsom, and D. J. Jarvis, "The electrical resistivity of gold films," Philosophical Transactions of the Royal Society of London. Series A, Mathematical and Physical Sciences **304**, 365–396 (1982).

[56]S. Dahal, A. Ali, J. W. Appel, T. Essinger-Hileman, C. Bennett, M. Brewer, R. Bustos, M. Chan, D. T. Chuss, J. Cleary, F. Colazo, J. Couto, K. Denis, R. Dünner, J. Eimer, T. Engelhoven, P. Fluxa, M. Halpern, K. Harrington, K. Helson, G. Hilton, G. Hinshaw, J. Hubmayr, J. Iuliano, J. Karakla, T. Marriage, J. McMahon, N. Miller, C. Nuñez, I. Padilla, G. Palma, L. Parker, M. Petroff, B. Pradenas, R. Reeves, C. Reintsema, K. Rostem, M. Sagliocca, K. U-Yen, D. Valle, B. Wang, Q. Wang, D. Watts, J. Weiland, E. Wollack, Z. Xu, Z. Yan, and L. Zeng, "Design and characterization of the Cosmology Large Angular Scale Surveyor (CLASS) 93 GHz focal plane," in *Millimeter, Submillimeter, and Far-Infrared Detectors and Instrumentation for Astronomy IX*, Society of Photo-Optical Instrumentation Engineers (SPIE) Conference Series, Vol. 10708, edited by J. Zmuidzinas and J.-R. Gao (2018) p. 107081Y, arXiv:1807.03927 [astro-ph.IM].

[57]K. Rostem, A. Ali, J. W. Appel, C. L. Bennett, A. Brown, M.-P. Chang, D. T. Chuss, F. A. Colazo, N. Costen, K. L. Denis, T. Essinger-Hileman, R. Hu, T. A. Marriage, S. H. Moseley, T. R. Stevenson, K. U-Yen, E. J. Wollack, and Z. Xu, "Silicon-based antenna-coupled polarization-sensitive millimeter-wave bolometer arrays for cosmic microwave background instruments," in *Proc. SPIE 9914, Millimeter, Submillimeter, and Far-Infrared Detectors and Instrumentation for Astronomy VIII*, edited by W. S. Holland and J. Zmuidzinas (International Society for Optics and Photonics, 2016) p. 99140D.

[58]E. J. Crowe, C. L. Bennett, D. T. Chuss, K. L. Denis, J. Eimer, N. Lourie, T. Marriage, S. H. Moseley, K. Rostem, T. R. Stevenson, D. Towner, K. U-Yen, and E. J. Wollack, "Fabrication of a silicon backshort assembly for waveguide-coupled superconducting detectors," IEEE Transactions on Applied Superconductivity **23** (2013), 10.1109/TASC.2012.2237211.

[59]J. Coonrod, "Choosing circuit materials for millimeter wave applications." High Frequency Electronics **12.7**, 22–30 (2013).

[60]Y. Tao and F. Scharf, "Revisiting the Effect of Nickel Characteristics on High-Speed Interconnect Performance," IEEE Transactions on Microwave Theory and Techniques **64**, 2447–2453 (2016).

[61]J. R. Claycomb and J. H. Miller, "Superconducting magnetic shields for SQUID applications," Review of Scientific Instruments **70**, 4562–4568 (1999).

[62]M. Hollister, H. McGregor, A. Woodcraft, D. Bintley, M. MacIntosh, and W. Holland, "Cryogenic magnetic shielding for SCUBA-2," (2008) p. 702023.

[63] S. Dahal, A. M. Ali, J. W. Appel, and T. Essinger-Hileman, "Design and characterization of the Cosmology Large Angular Scale Surveyor (CLASS) 93 GHz focal plane," in *Submitted to Proceedings of the SPIE* (2018).

[64] Y. Li, J. E. Austermann, J. A. Beall, S. M. Bruno, S. K. Choi, N. F. Cothard, K. T. Crowley, S. M. Duff, P. A. Gallardo, S. W. Henderson, S.-P. P. Ho, J. Hubmayr, B. J. Koopman, J. J. McMahon, M. D. Niemack, M. Salatino, S. M. Simon, S. T. Staggs, J. R. Stevens, J. N. Ullom, J. Ward, and E. J. Wollack, "Performance of the advanced ACTPol low frequency array," https://doi.org/10.1117/12.2313942 **10708**, 16–24 (2018).

[65] Y. Li, J. E. Austermann, J. A. Beall, S. M. Bruno, S. K. Choi, N. F. Cothard, K. T. Crowley, S. M. Duff, S. P. P. Ho, J. E. Golec, G. C. Hilton, M. Hasselfield, J. Hubmayr, B. J. Koopman, M. Lungu, J. McMahon, M. D. Niemack, L. A. Page, M. Salatino, S. M. Simon, S. T. Staggs, J. R. Stevens, J. N. Ullom, E. M. Vavagiakis, Y. Wang, E. J. Wollack, and Z. Xu, "In Situ Performance of the Low Frequency Array for Advanced ACTPol," IEEE Transactions on Applied Superconductivity **31** (2021), 10.1109/TASC.2021.3063334, arXiv:2101.02658.

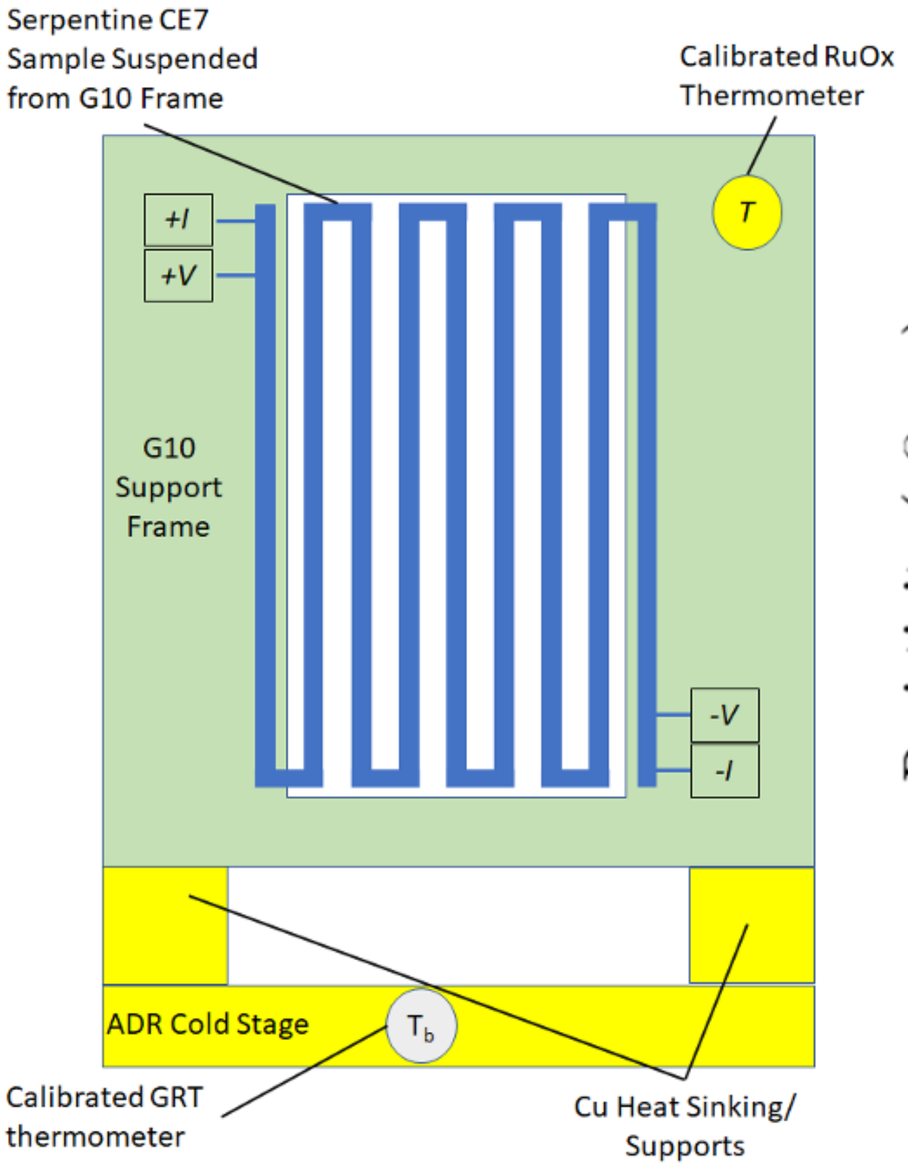
Serpentine CE7
Sample Suspended
from G10 Frame
Calibrated RuOx
Thermometer
+I
+V
T
G10
Support
Frame
-V
-I
ADR Cold Stage
T_b
Calibrated GRT
thermometer
Cu Heat Sinking/
Supports

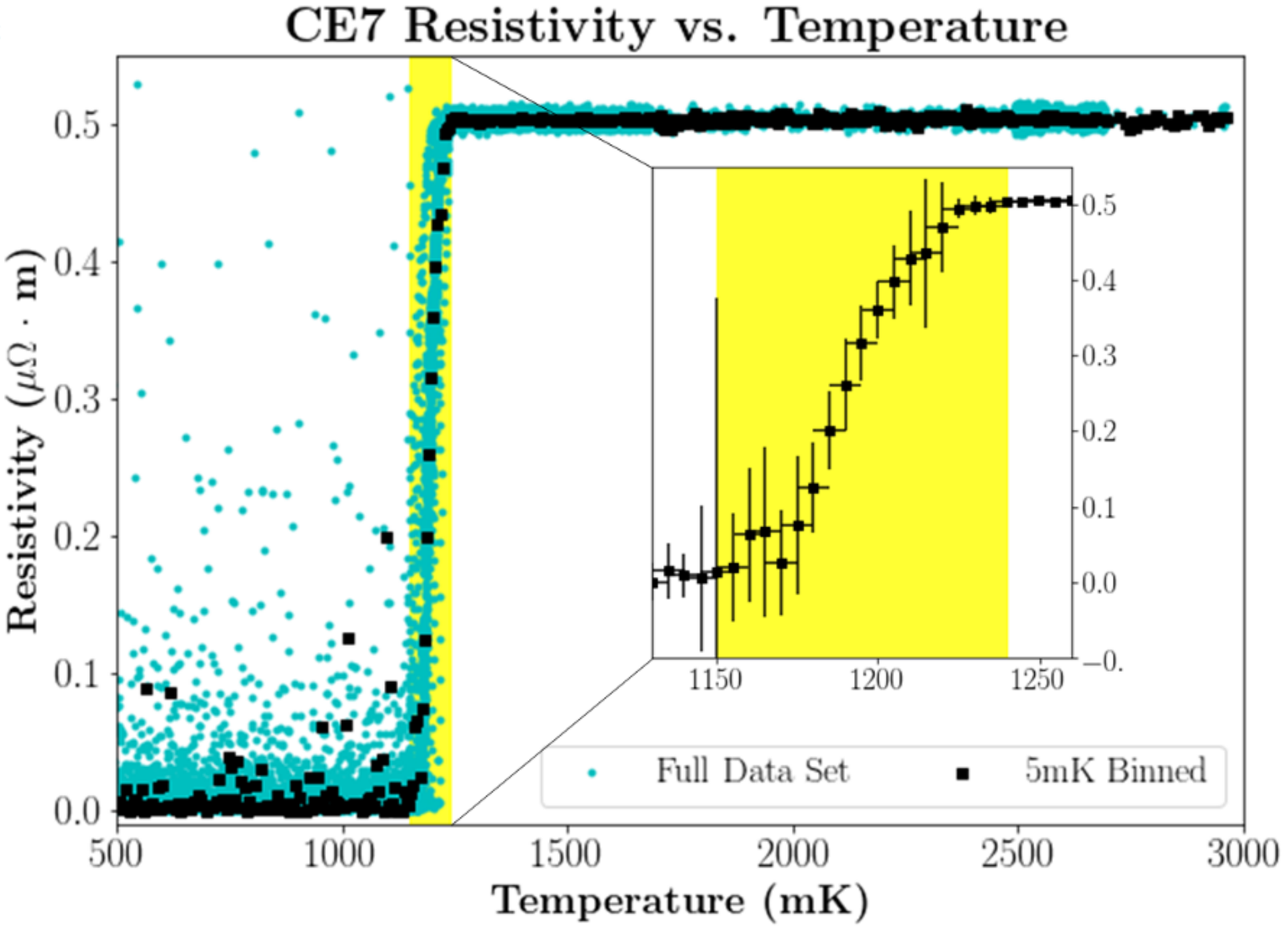
CE7 Resistivity vs. Temperature
Resistivity ($\mu\Omega \cdot$ m)
Temperature (mK)
0.0
0.1
0.2
0.3
0.4
0.5
500
1000
1500
2000
2500
3000
1150
1200
1250
−0.
Full Data Set
5mK Binned

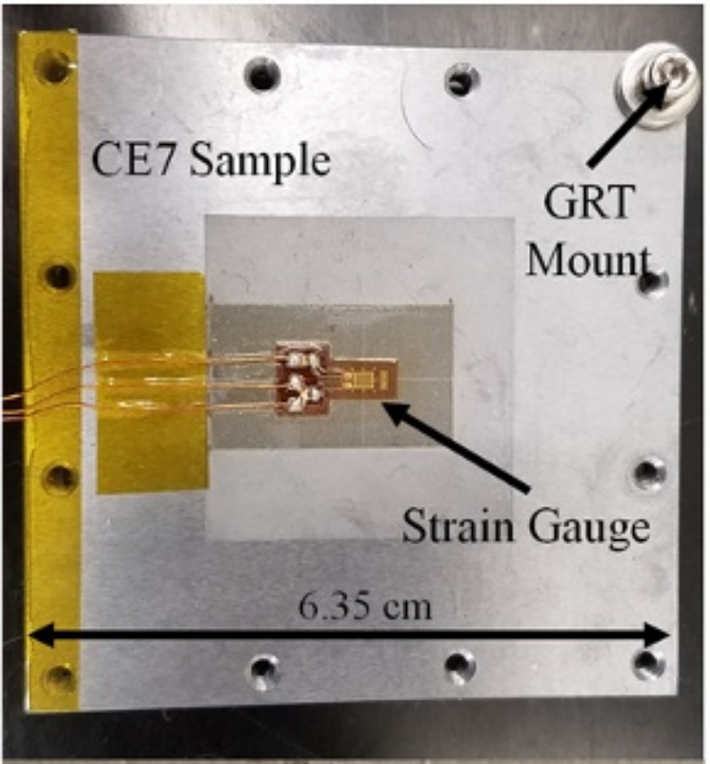
CE7 Sample
GRT
Mount
Strain Gauge
6.35 cm

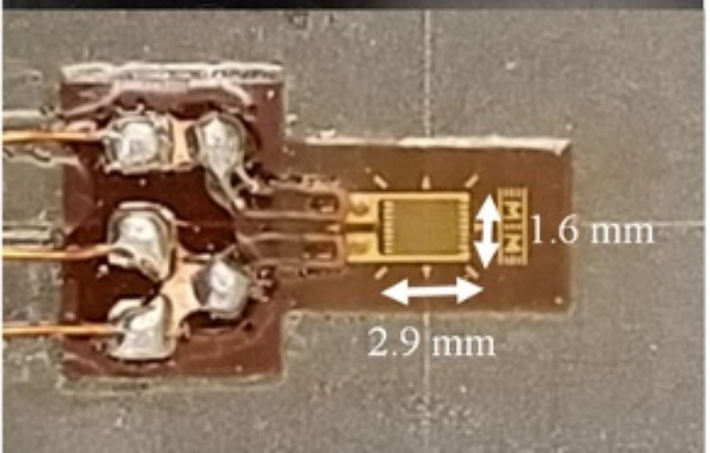
1.6 mm
2.9 mm

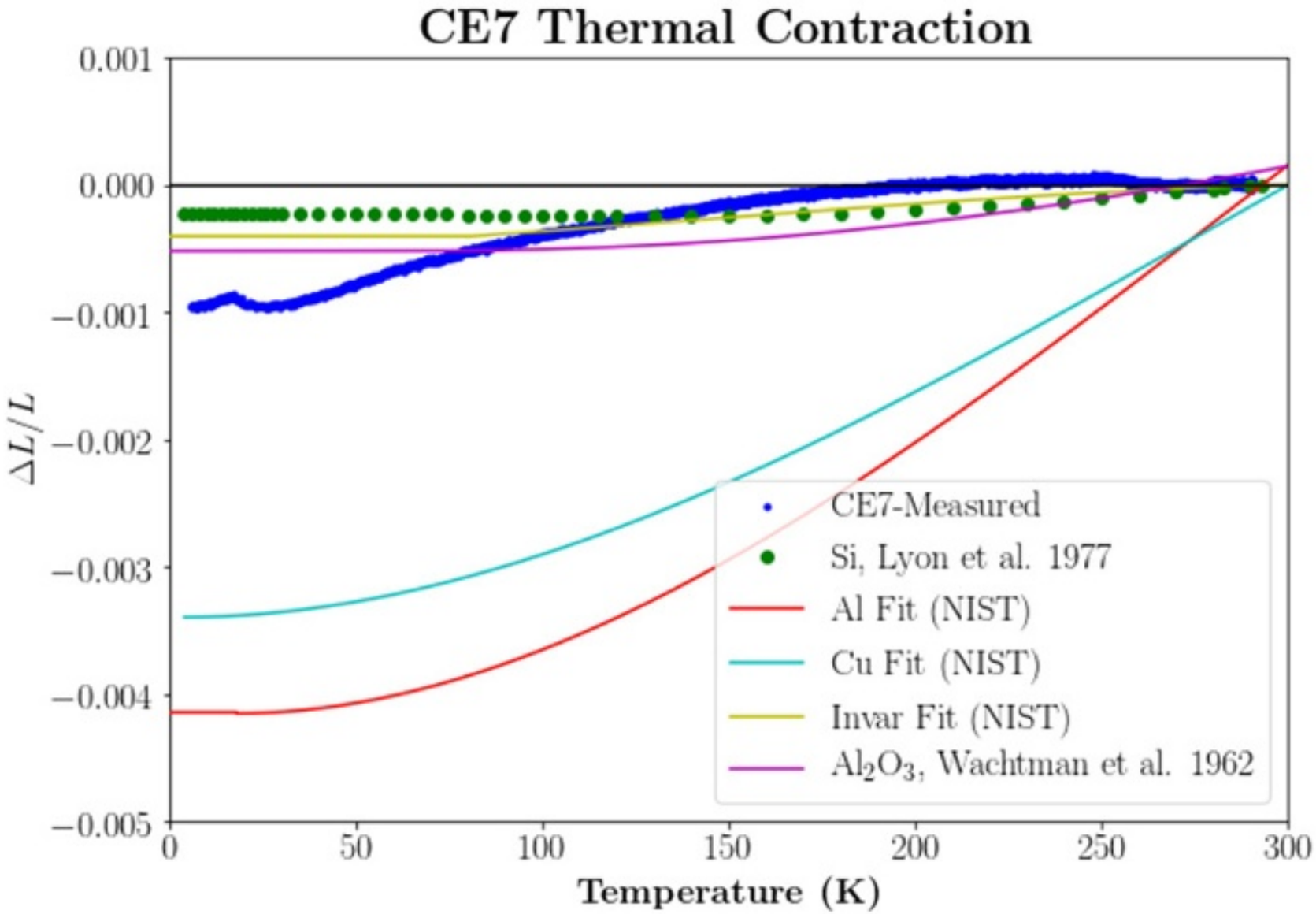
CE7 Thermal Contraction
0.001
0.000
−0.001
−0.002
−0.003
−0.004
−0.005
ΔL/L
0
50
100
150
200
250
300
Temperature (K)
CE7-Measured
Si, Lyon et al. 1977
Al Fit (NIST)
Cu Fit (NIST)
Invar Fit (NIST)
Al2O3, Wachtman et al. 1962

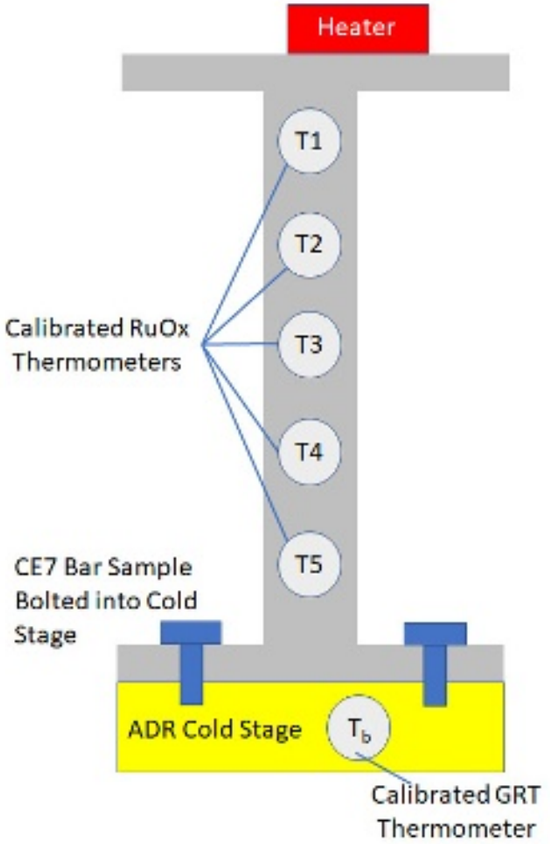
Heater
T1
T2
T3
T4
T5
Calibrated RuOx Thermometers
CE7 Bar Sample Bolted into Cold Stage
ADR Cold Stage
T_b
Calibrated GRT Thermometer

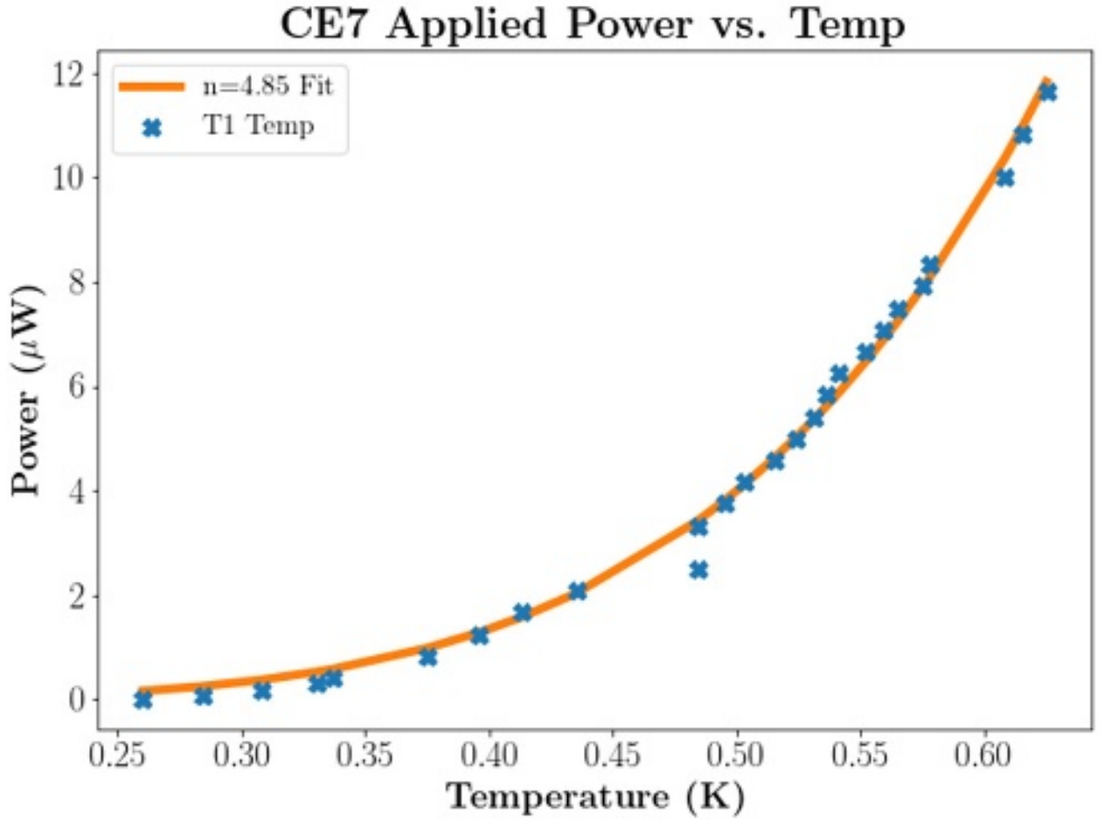
CE7 Applied Power vs. Temp
n=4.85 Fit
T1 Temp
Power (μW)
Temperature (K)
0
2
4
6
8
10
12
0.25
0.30
0.35
0.40
0.45
0.50
0.55
0.60

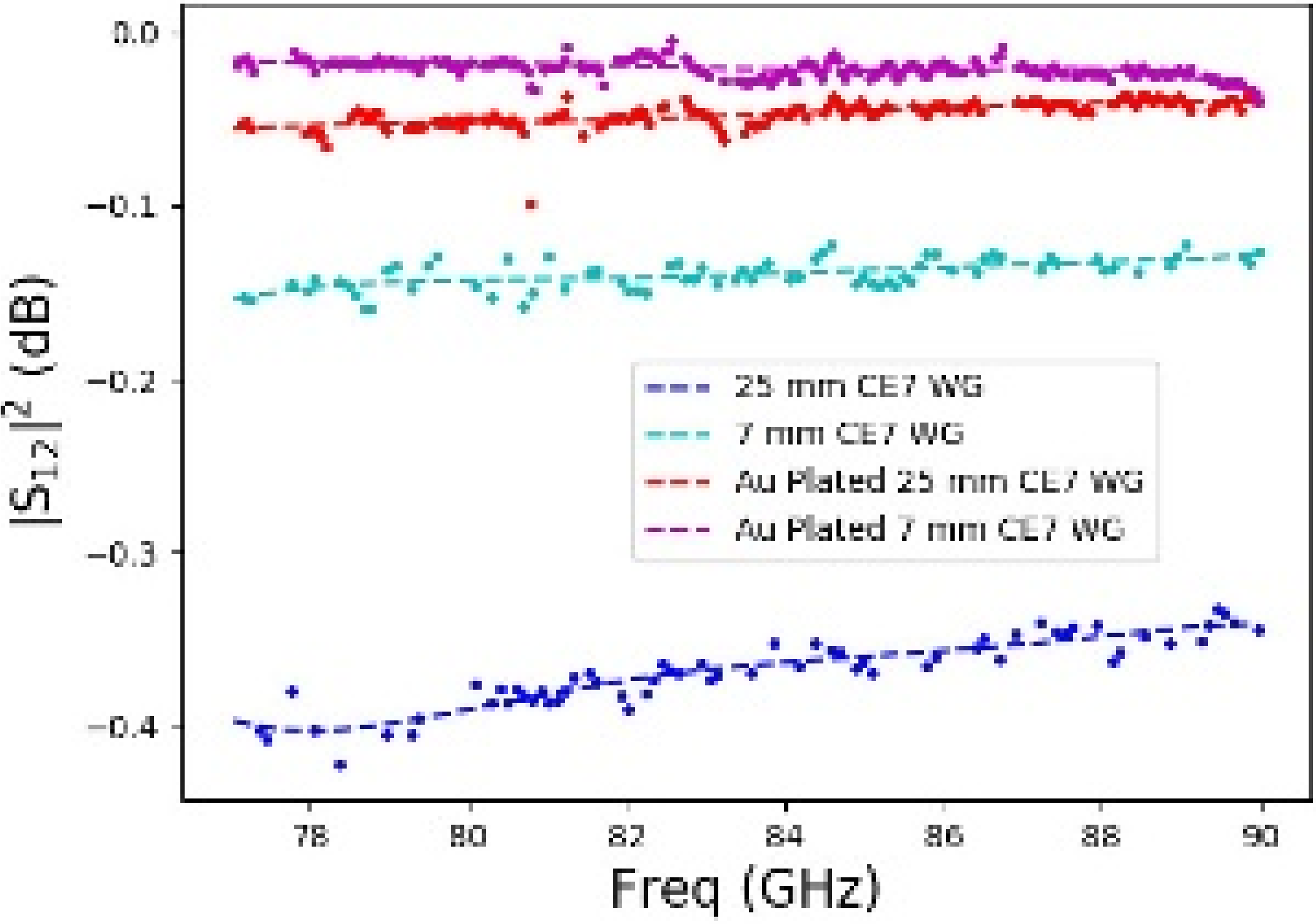
0.0
−0.1
−0.2
−0.3
−0.4
$|S_{12}|^2$ (dB)
78
80
82
84
86
88
90
Freq (GHz)
25 mm CE7 WG
7 mm CE7 WG
Au Plated 25 mm CE7 WG
Au Plated 7 mm CE7 WG

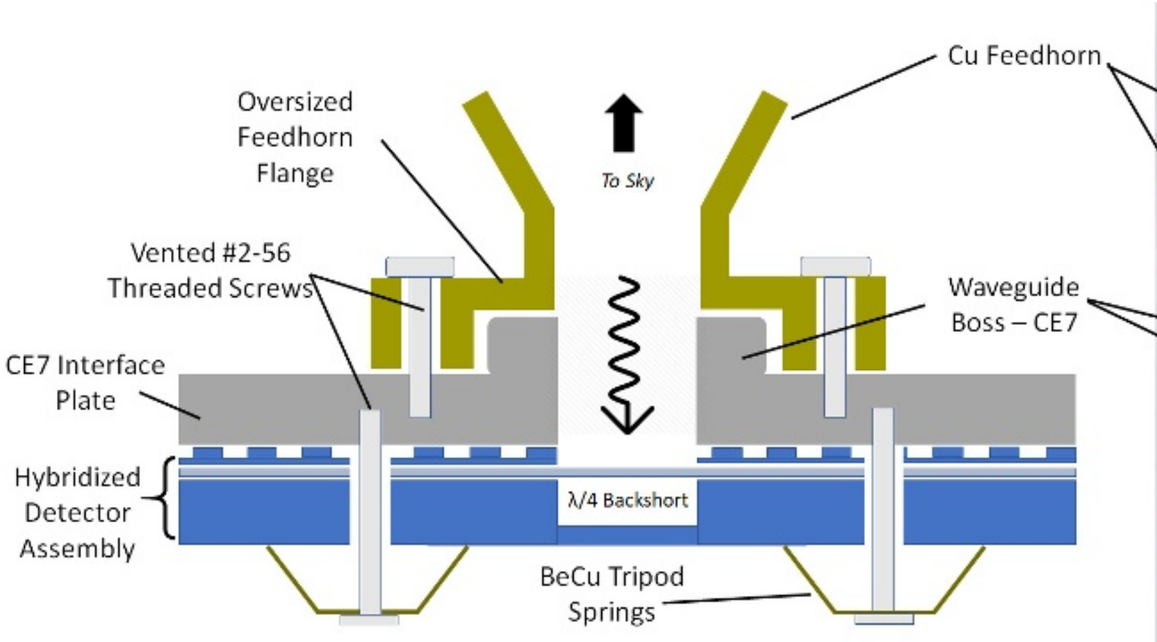
Oversized
Feedhorn
Flange
To Sky
Cu Feedhorn
Vented #2-56
Threaded Screws
Waveguide
Boss – CE7
CE7 Interface
Plate
Hybridized
Detector
Assembly
λ/4 Backshort
BeCu Tripod
Springs

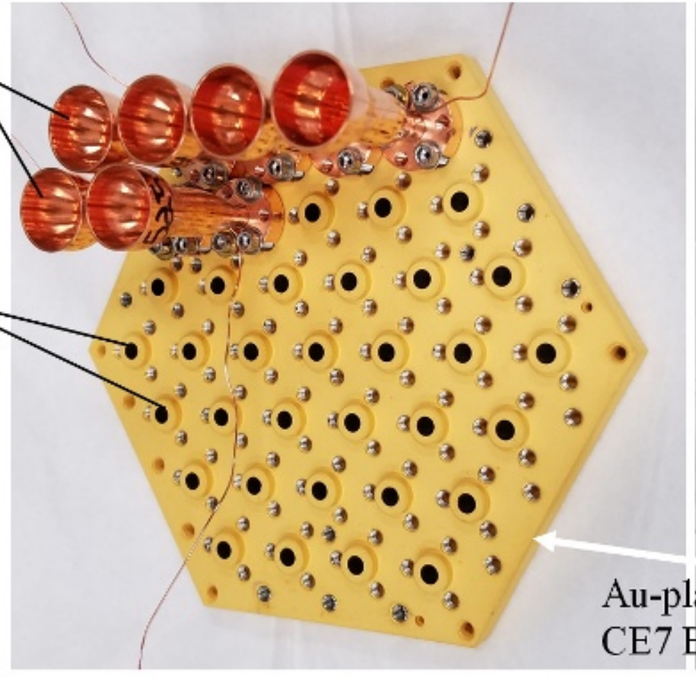
Au-plated
CE7 Baseplate

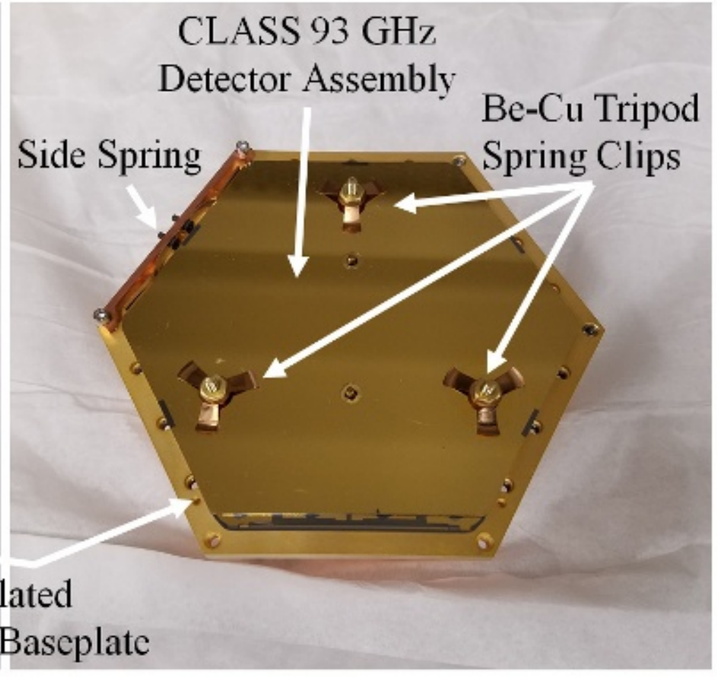
CLASS 93 GHz
Detector Assembly
Side Spring
Be-Cu Tripod
Spring Clips

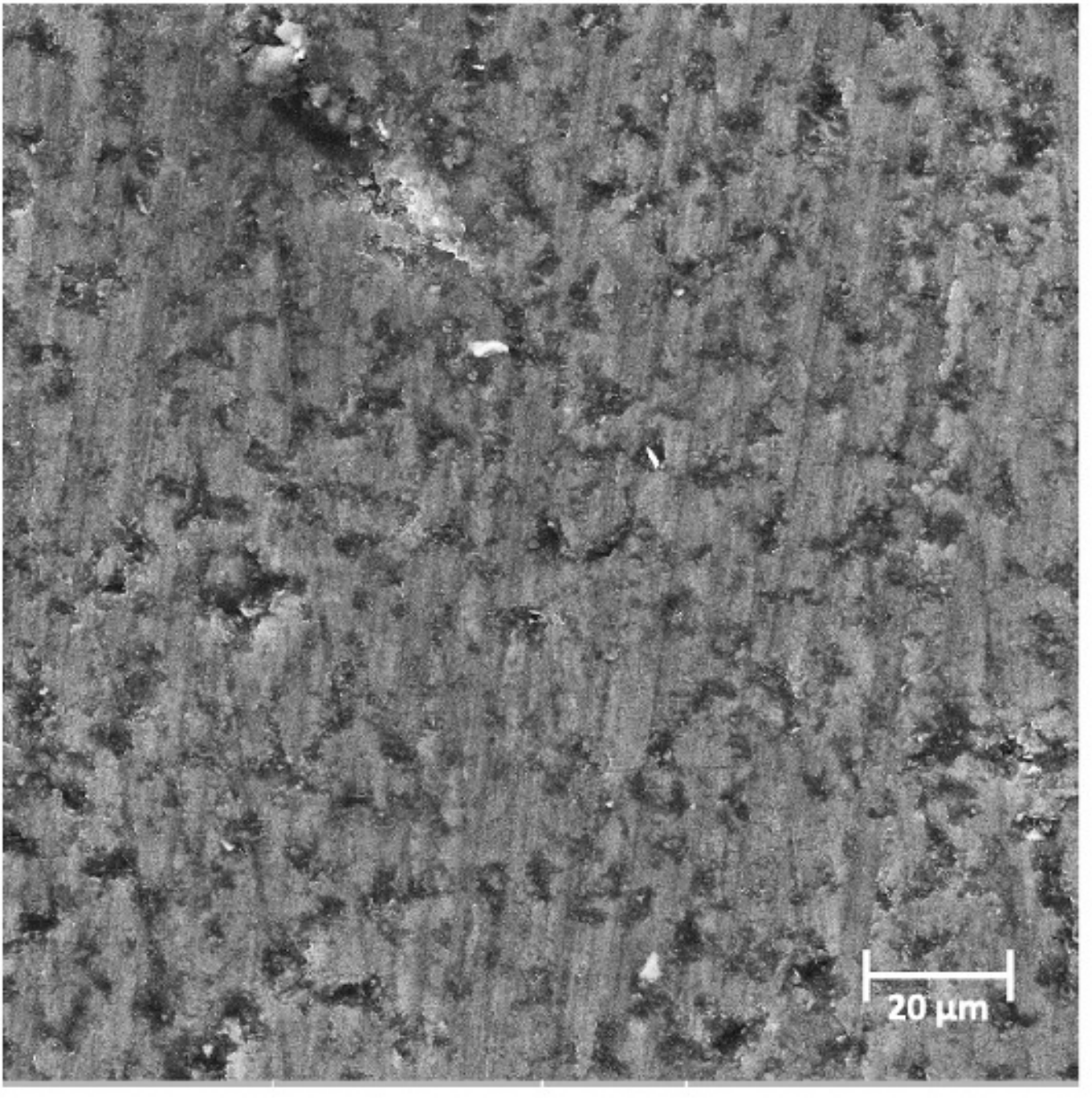
20 µm

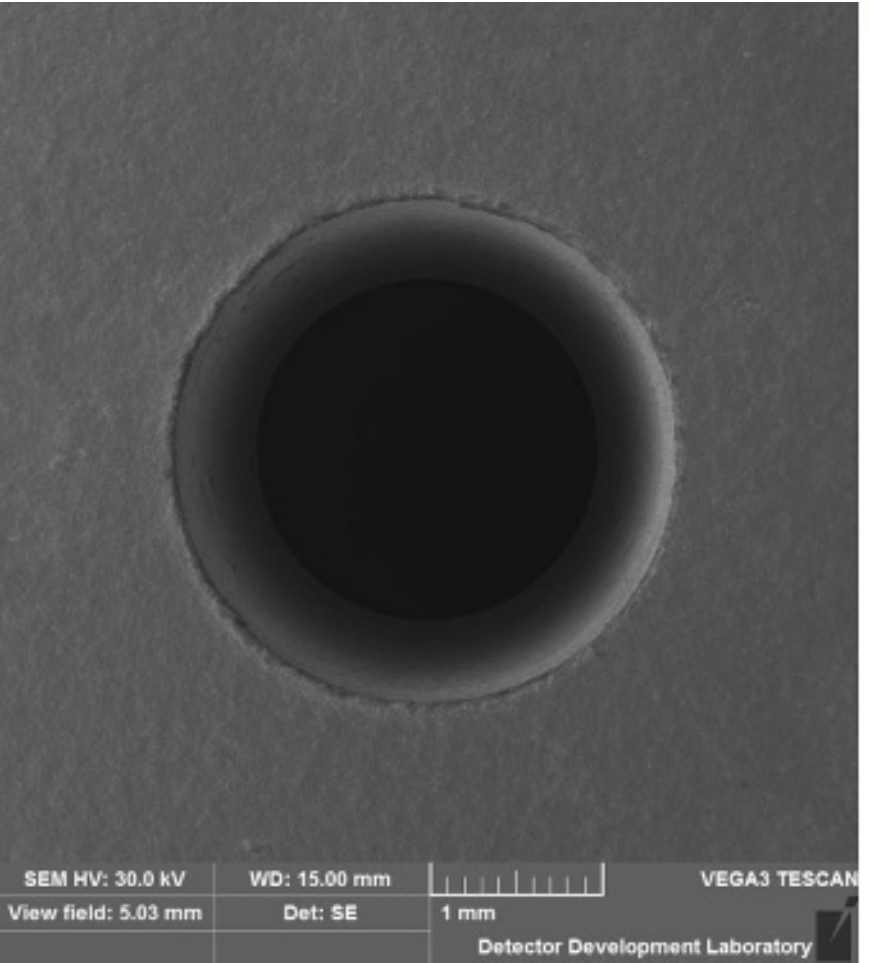
SEM HV: 30.0 kV
WD: 15.00 mm
VEGA3 TESCAN
View field: 5.03 mm
Det: SE
1 mm
Detector Development Laboratory

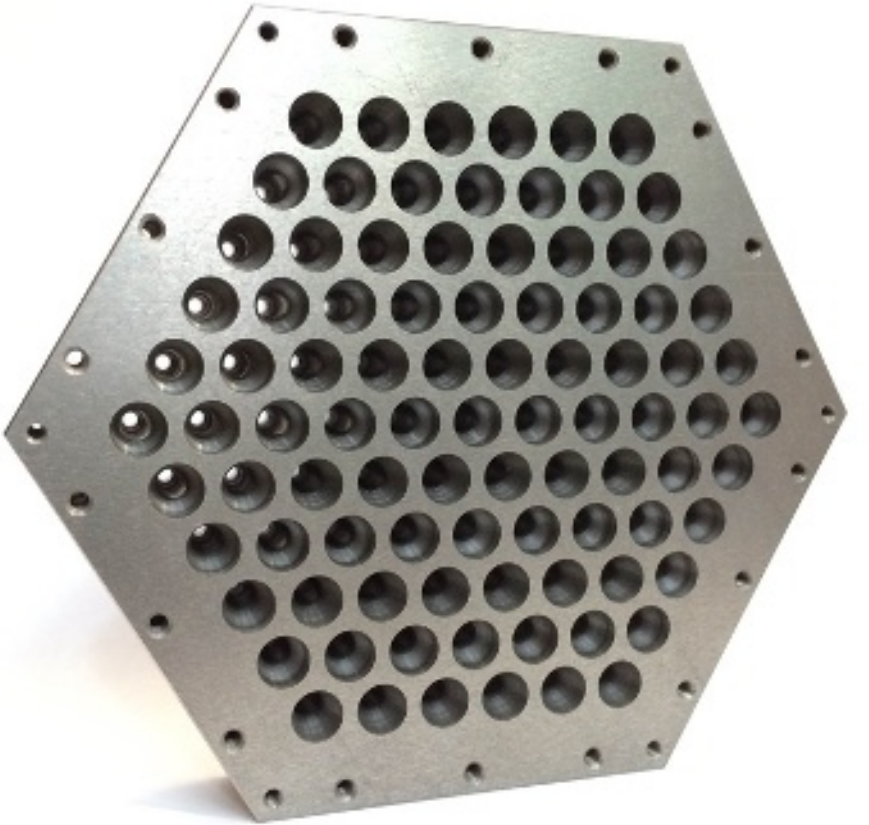

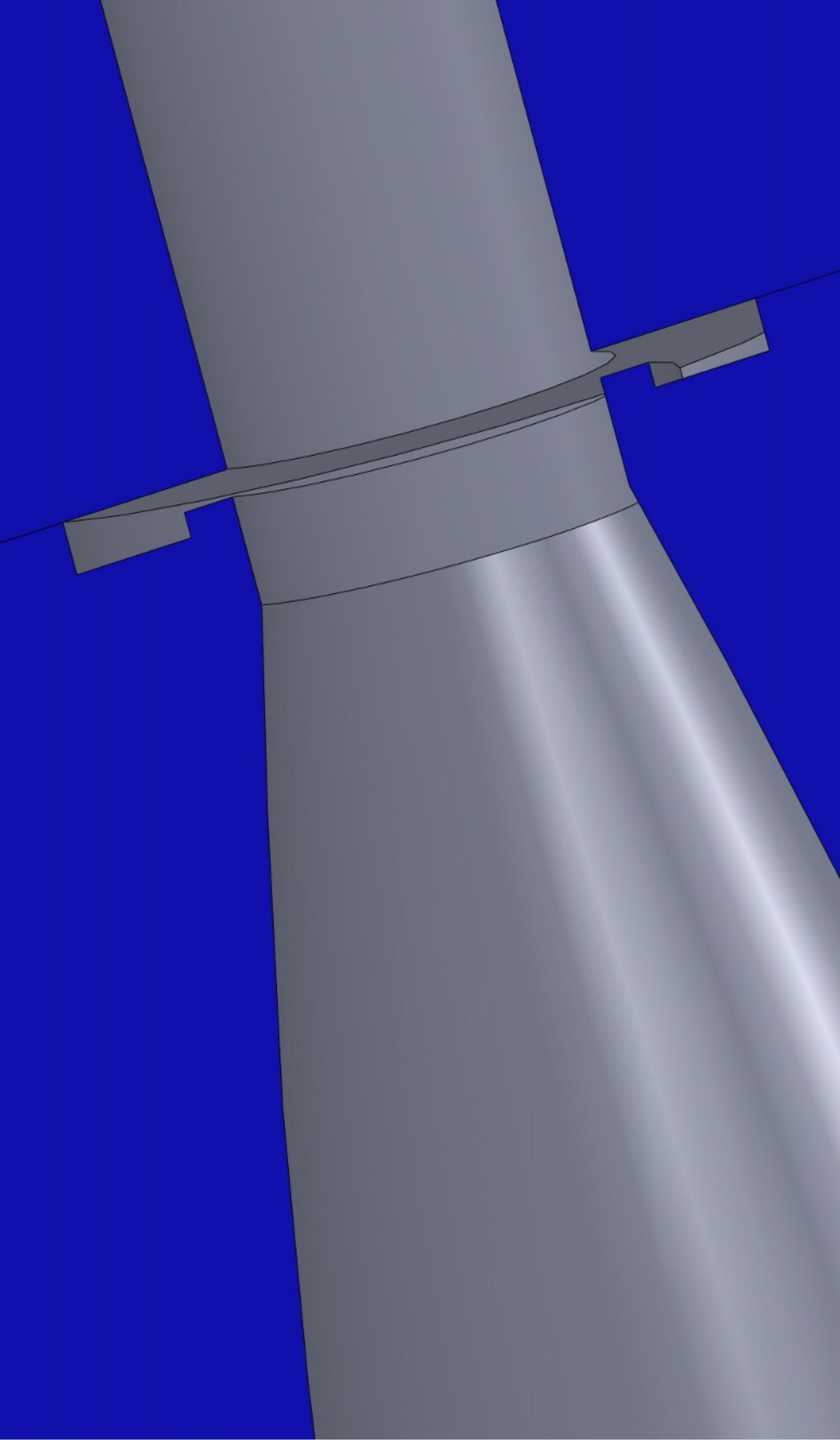

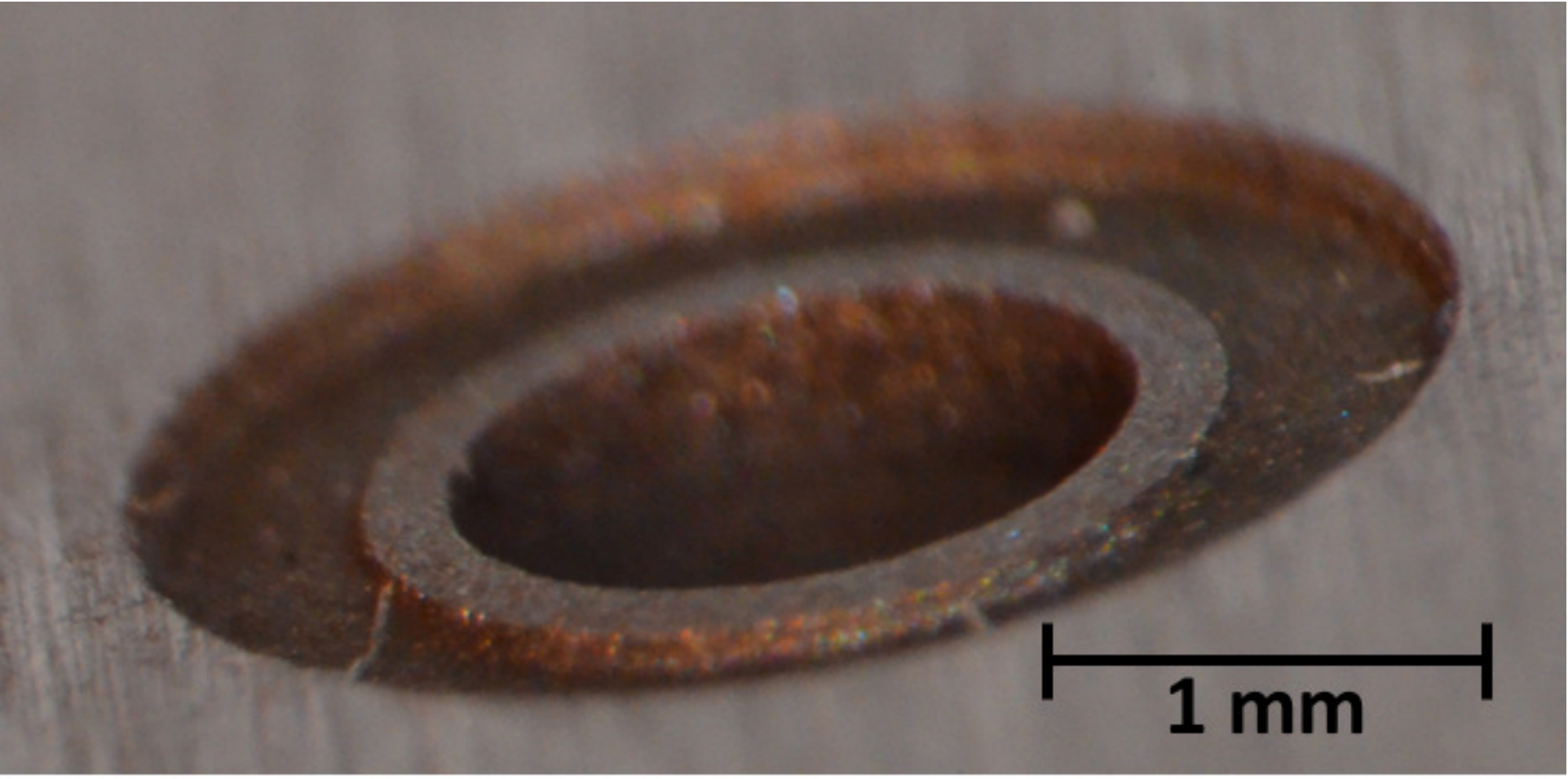
1 mm